System on a Chip

Interim Progress Report
June 1998

Prepared by: Linda P.B. Katehi

During the month of May the University of Michigan group was formed and its membership was finalized. The group structure and the distribution of tasks are shown below.

Prof. Linda P.B. Katehi (PI/PD)		
Filters and Diplexers	**Switches**	**SSPA**
Prof: **Linda P.B. Katehi**	Prof: **Gabriel M. Rebeiz**	Prof: **Pallab Bhattacharya**
Students: Lee Harle	Student: Jeremy Moldavin	Student: J-S Rhieh
Tom Schwarz	Prof: Linda P.B. Katehi	Jack Ma
	Student: Sergio Pacheco	Prof. Linda P.B. Katehi
		Student: Kevin Lu

In terms of effort in each task our status is outlined below:

Filters and Diplexers

During the past year and a half we have accomplished the design of a single cavity Si micromachined filter. An extensive study of this filter is given in Appendices I and II. Our accomplishments during May and the goals for the following month are given below:

- *Accomplishments During the Month of May*

A number of fabrication issues have been resolved. Specifically, the resonators have been fabricated on Si wafers with a Si_3N_4 layer as a masking medium. LPCVD Si_3N_4 was chosen over LPCVD SiO_2 due to its better quality. The presence of silicon nitride may introduce additional losses on the input and output lines. To characterize loss performance calibration standards were fabricated on PECVD nitride in order to characterize line loss. The results have shown that the presence of silicon nitride influences loss very little to the point that it is not taken into account. Furthermore, we have identified a lumped element model for a multicavity filter and we are in the process of parametrizing the various geometrical components of the filter structure including the cavities and the coupling slots. Having these macromodels available we can then use a simple synthesis technique to specify the geometrical parameters appropriate for an desired filter performance.

- *Goals for the Month of June*

During this month we plan to complete the parametrization of the filter design and specifically the parametrization of the coupling slots. The coupling slots will be represented by admittance inverters to allow for the design of a bandpass filter through a low-pass prototype design. With this accomplished we can then analyze a given design by a full-wave technique (HFSS) to understand and evaluate the maximum possible filter rejection. In this planar design this filter rejection is expected to be limited by the excitation of a surface wave noise in the substrate.

Switches

We have developed single pole, single throw switches with activation voltages between 12V and 16V. These are three-electrode switches whose operation is extensively described in Appendix III. The isolation is these switches is better than –30 dB and the insertion loss is less than 0.1 dB for operating frequencies up to 40 GHz. A different type of a switch has been also considered and results from this study are shown in Appendix VI.

- *Accomplishments during the Month of May*

During this month we experimented with polyamide as a sacrificial layer. The advantages of this material are its capability to planarize the top electrodes. This has direct impact on the capability to reduce the stress on the evaporated metals and optimize the integrity of the switch structure. This material was the first one to be used as a sacrificial layer but we had problems removing it effectively from areas underneath the electrodes. During this past month, the fabrication process has been optimized to allow for an easy removal of the sacrificial layer. A new set of switches has been developed. This set includes two-electrode switches and not three electrodes ones. This was done to reduce the fabrication steps during the development of the sacrificial layer process.

- *Goals for the Month of June*

During the month of June we will apply the developed process on three-electrode switches. During this process we will also try to optimize the use of paraline as a dielectric layer. So far paraline has been utilized but we do not have absolute control over the thickness of the deposited dielectric. The development of a repeatable process of paraline deposition along with the development and measurement of a three-electrode switch will be our main effort during this month.

SiGe SSPA

During the past year we have accomplished a number of goals. Specifically, we have developed a SiGe/Si npn 5μ x 5μ HBT technology. The devices show current gain of 200, f_T at 28GHz, f_{max} at 52 GHz, base ideality factor 1.79 and collector ideality factor 1.04. Furthermore, SiGe/Si HBT microwave monolithic amplifiers at X and Ku bands have been fabricated and show 4 dB of gain/stage at 10 GHz, 1.4 dB gain/stage at 17

GHz respectively. X-band two and three-stage amps show 5.7 dB and 12.6 dB gain at 10 GHz. The results of this work are described in Appendix V.

- *Accomplishments for the Month of May*

During this past month we have focused our efforts on improving the yield and f_T/f_{max} of the above devices. We have observed that during fabrication there is an unknown thin layer developed between the base metal and the base thus deteriorating device performance. Measurement of base/collector characteristics in these devices demonstrates a performance of a back-to-back diode. A number of fabrication runs were performed to identify the problem and extensive measurements confirm the presence of this layer.

- *Goals for the Month of June*

During this coming month we plan to spend all of our effort correcting identified problem. We plan to change the sequence of some fabrication steps to eliminate the development of this layer. An extensive description of the fabrication process will be provided in the June report.

Appendix I

Si-Micromachined Cavity Filters

A Micromachined High-Q X-Band Resonator

John Papapolymerou, Jui-Ching Cheng, Jack East, *Member, IEEE*, and Linda P. B. Katehi, *Fellow, IEEE*

Abstract— **This letter presents a new structure which can be used as a microwave high-Q resonator for the development of narrow-band low-loss filters in a planar environment. The resonator is made of a low-loss micromachined cavity which is easy to integrate with monolithic circuits. Compared to conventional metallic resonators, the performance of this resonator is similar, but the weight and size are significantly reduced.**

I. Introduction

CONVENTIONAL microwave high-Q resonators made by metallic rectangular or cylindrical waveguides are heavy in weight, large in size, and costly to manufacture. Furthermore, they do not allow for an easy integration with monolithic integrated circuits.

With the maturity of micromachining techniques in fabricating microwave circuits, it is now possible to make miniature silicon micromachined waveguides or cavities [1]–[4] as building blocks for the development of high-Q bandpass filters. The quality factor that can be achieved with this technique is much higher than the quality factor of traditional microstrip resonators either printed on a dielectric material or suspended in air with the help of a dielectric membrane [5]. A possible high-Q filter geometry is shown in Fig. 1, consisting of input and output microstrip lines and rectangular cavities on different dielectric layers. The cavities are made by Si micromachining and are metallized by conventional techniques. Coupling between the cavities and microstrip lines is achieved via the slots etched at appropriate locations with respect to the microstrip lines. Coupling between cavities is controlled by the size, position, and orientation of the corresponding coupling slots. The vertical stacking of the cavities greatly reduces the occupied area when multiple cavities are needed for filter design.

In the following sections, a micromachined resonator is analyzed and built. The theoretically calculated results are compared to measurements. The Q of the resonator is computed and compared to the Q of conventional metallic and planar resonators.

II. Theoretical Analysis

A hybrid technique [6] that combines the method of moments (MoM) and the finite-element method (FEM) is used in the theoretical analysis. This technique primarily uses the method of moments to analyze the open part of the structure and the FEM to compute the fields inside the cavity. The two techniques are coupled at the slot surface. Due to the flexibility of FEM, the shape of the cavity is not restricted to be rectangular and the cavity can be filled with complex material. The procedure of applying this technique is briefly described in the next paragraph. The exact formulation will not be shown here, since it is similar to the one presented in [6].

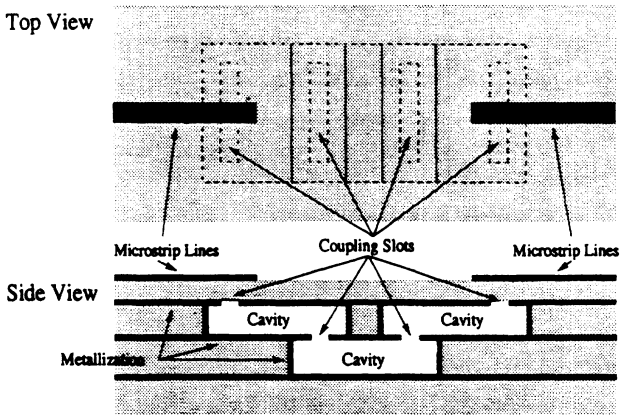

Fig. 1. The structure of the proposed micromachined bandpass filters.

Fig. 2 shows a cavity coupled by two microstrip lines through two slots. By using the equivalence principle, the slots can be replaced by perfect electric conductors with equivalent magnetic currents flowing above their surface at the location of the slots. In this way, the cavity and the microstrip lines are separated by the ground plane of the microstrip lines. The field inside or outside the cavity can be represented as an integral of the unknown equivalent current sources dot-multiplied by the dyadic Green's function. By enforcing the continuity of tangential magnetic fields across the slots and using Galerkin's method, a matrix equation linking the unknown current distribution on the microstrip lines and field distribution on the slots is derived. The finite element technique applied in the cavity links the fields on the two slots through an FEM matrix. This hybrid technique reduces to a matrix equation which is then solved to compute the unknown current and field distributions.

III. Fabrication

The X-band resonator is fabricated using standard micromachining techniques. For the circuit shown in Fig. 2 two silicon wafers, 500-μm thick, with 1.45-μm thermally grown oxide deposited on both sides are used. To measure the resonator with on-wafer probing, a coplanar waveguide (CPW)-to-microstrip transition is incorporated to provide a matched transition to the feeding lines. The ground of the CPW and the microstrip are set at an equal potential with the implementation of via holes. The characteristic impedance of

Manuscript received January 21, 1997. This work was supported by the Army Research Office (MURI Program) under Contract DAAH-04-96-1-0001.

The authors are with the Department of Electrical Engineering and Computer Science, The University of Michigan, Ann Arbor, MI 48019-2122 USA.

Publisher Item Identifier S 1051-8207(97)03854-3.

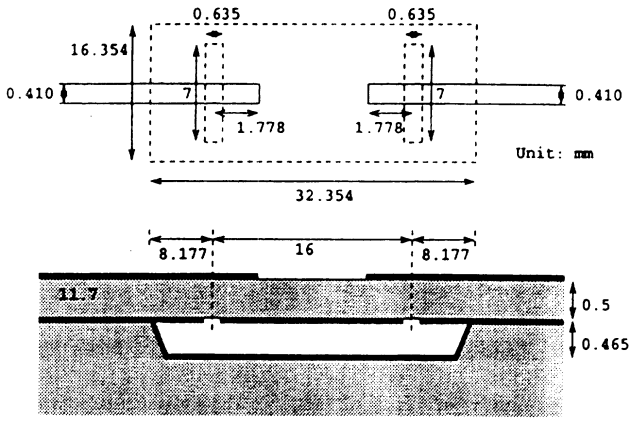

Fig. 2. An X-band micromachined resonator.

both the CPW and microstrip is 50 Ω. The two microstrip lines are gold electro-plated with a total thickness of 7.5 μm in order to minimize losses. Infrared alignment is used in order to correctly align the two slots on the back of the wafer with the microstrip lines printed on the other side.

The cavity is fabricated on a second wafer by using chemical anisotropic etching (EDP or TMAH) until a depth of about 465 μm is achieved. Once the wafer is etched, it is metallized with a total thickness of 2 μm. The two wafers are then bonded together with silver epoxy that is cured at 150 °C. The alignment between the two wafers is achieved by opening windows on the top wafer during the etching process to align to marks that are placed on the second wafer.

IV. Computed and Measured Results

A resonator with the dimensions shown in Fig. 2 is built and the S-parameters are measured and compared with the computed results. The reference planes for the measurement are at the middle of the slots and de-embedding is achieved using a thru-reflect-line (TRL) calibration with the standards fabricated on the same wafer. Computed and measured results can be seen in Fig. 3. Note that although the cavity is not rectangular, we find that the first resonant frequency is very close to that of a rectangular cavity of similar size. The small difference (1%) in the center frequency is partly due to the finite accuracy in modeling the nonvertical slopes of the cavity and partly to the inherent numerical error of our simulation technique. Fig. 4 shows the z-component electric field density on the bottom of the cavity at the resonant frequency (10.4 GHz). The field pattern also matches quite well to that of the first resonant mode of a rectangular cavity of the similar size. The figure is drawn according to the physical dimension of the cavity. The two coupling slots are located at 1/4 and 3/4 of the length of the cavity as indicated in the figure.

In order to evaluate the unloaded Q (Q_u) of the cavity the losses due to the excess length of the lines from the reference planes, which is needed to tune the slots, must be removed. For this reason the ohmic loss on the feeding lines is found from the TRL standards and is used to compute the loss on the two open end stubs extending beyond the center of the slots. For the measured results shown in Fig. 3 this loss has already been de-embedded. The loaded Q (Q_l) of the cavity defined as

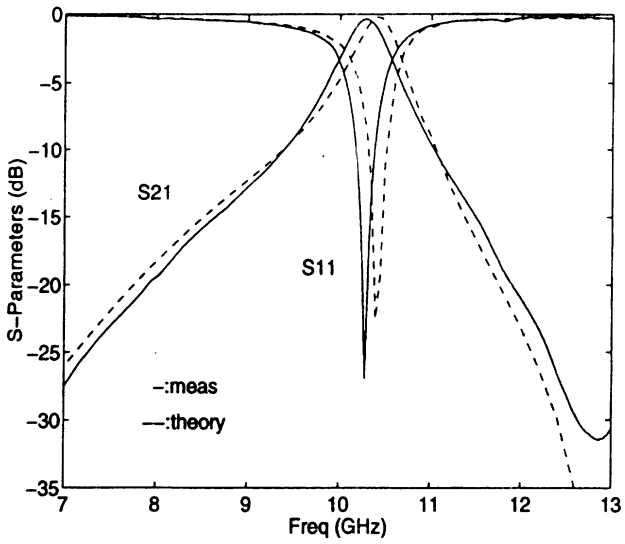

Fig. 3. Measured and theoretical S-parameters for the resonator of Fig. 2.

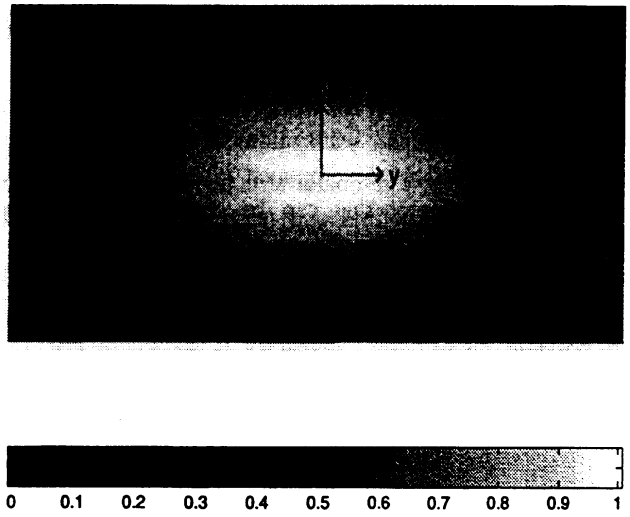

Fig. 4. Computed z-component of the electric field density on the bottom of the cavity.

$$Q_l = \frac{f_o}{\Delta f_{3-\mathrm{dB}}} \tag{1}$$

where f_o = 10.285 GHz is the resonant frequency and $\Delta f_{3-\mathrm{dB}}$ = 0.5 GHz is the 3-dB bandwidth, is found equal to 20.57. The external Q of the resonator Q_e, which includes the input–output loading effects, can be found from [5]

$$S_{21}\,(\mathrm{dB}) = 20\log_{10}\left(\frac{Q_l}{Q_e}\right) \tag{2}$$

where S_{21} was measured to be 0.36 ± 0.04 dB. The error is attributed to calibration accuracy and fabrication tolerances. Equation (2) gives $Q_e = 21.44 \pm 0.1$. Knowing Q_e and Q_l we can find Q_u from the known relation

$$\frac{1}{Q_l} = \frac{1}{Q_u} + \frac{1}{Q_e}. \tag{3}$$

Using the above definitions and the measured results, Q_u is found to be equal to 506 ± 55 and is very close to the

TABLE I
COMPARISON OF MEASURED Q FOR SEVERAL RESONATORS AT X-BAND

type		size (mm x mm x mm)	Q_u
non-planar	metal (rectangular)	19.8x22.9x10.2	8119
	metal (rectangular)	16x32x0.465	526
planar	micromachined cavity	16x32x0.465	506
	membrane-microstrip	5.3x7.1x0.35	234
	microstrip	2.65x3.55x0.5	125

theoretical value of 526 for a metallic cavity with the same dimensions [7].

The advantages of the proposed micromachined cavity are made clear by the comparisons of Table I (for the first cavity see [8]). As seen by this table, the micromachined cavity has a Q similar to a metallic waveguide cavity with the same dimensions, but it has the advantage of maintaining a planar form that allows for easy integration with microwave integrated circuit (MIC) and monolithic MIC (MMIC) structures. Despite its planar character, the micromachined cavity has a Q that is four times higher than that of traditional microstrip resonators ($Q_u = 125$).

V. CONCLUSION

In this letter, a new resonator structure consisting of input and output microstrip lines and micromachined rectangular cavities is presented. The use of Si micromachining enables the integration of a cavity resonator with microstrip components without affecting the planar character of the circuit. The size and weight of this component is significantly reduced compared to conventional resonators made by metallic cavities, while demonstrating an increased quality factor when compared with other planar resonators. We should note here that this high-Q resonator can be used as a basic element in the design and fabrication of high-Q bandpass filters.

REFERENCES

[1] R. F. Drayton and L. P. B. Katehi, "Microwave characterization of microshield lines," in *Dig. 40th ARFTG Conf.*, Orlando, FL, Dec. 1992.
[2] ——, "Experimental study of micromachined circuits," in *Dig. 1993 Int. Symp. Space Terahertz Tech.*, Los Angeles, CA, Mar. 1993.
[3] ——, "Micromachined circuits for MM-wave applications," in *Dig. 1993 Euro. Microwave Conf.*, Madrid, Spain, Sept. 1993.
[4] R. F. Drayton, T. M. Weller, and L. P. B. Katehi, "Development of miniaturized circuits for high-frequency applications using micromachining techniques," *Int. J. Microcirc. Elec. Packaging*, vol. 3, 1995.
[5] C. Y. Chi, "Planar microwave and millimeter-wave components using micromachining technologies," Ph.D. dissertation, Univ. of Michigan, Ann Arbor, 1995.
[6] J. Cheng, N. I. Dib, and L. P. B. Katehi, "Theoretical modeling of cavity-backed patch antennas using a hybrid technique," *IEEE Trans. Antennas Propagat.*, vol. 43, pp. 1003–1013, Sept. 1995.
[7] R. E. Collin, *Foundations for Microwave Engineering*. New York: McGraw-Hill, 1966, pp. 322–325.
[8] K. Chang, *Handbook of Microwave and Optical Components-Volume I*. New York: Wiley, 1989, pp. 196–199.

Appendix II

The Effects of the Position of the Coupling Slot on Filter Performance

Submitted to the 1998 European Microwave Conference

The effects of slot positioning on the bandwidth of a micromachined resonator

Lee Harle, John Papapolymerou, Jack East and Linda P.B. Katehi
Department of Electrical Engineering and Computer Science
The University of Michigan, 1301 Beal Avenue
Ann Arbor, MI 48109-2122

Abstract

This paper presents the effect of slot positions on the bandwidth and the response of a micromachined high-Q X-Band resonator formed by a micromachined cavity. Theory and experiment indicate that a narrow-band, low-loss response can be achieved by changing the placement of the slots relative to the center of the cavity. As a result, narrow-band, low-loss, monolithic filters with small weight and planar characteristics can be designed.

I Introduction

Microwave high-Q resonators are traditionally made of metallic rectangular or cylindrical waveguides that are heavy in weight, costly to manufacture and difficult to integrate with monolithic circuits. Recently it has been shown [1] that a low-loss, high-Q resonator can be fabricated in a planar environment by using standard micromachining techniques [2]. The X-Band resonator shown in Fig. 1 consists of input and output microstrip lines that reside on top of a silicon wafer and couple energy into a micromachined cavity which is formed on a second wafer via slots. The energy that is inserted in the cavity can travel through it in the form of a propagating or evanescent wave. Measurements have shown an insertion loss of 0.36 dB and an unloaded quality factor Q_u of 506 that is in good agreement with the theoretical value of a rectangular metallic cavity of similar size [3]. This resonator can be used as a building element for the design and fabrication of narrow-band, low-loss filters and multiplexers made of multiple cavities of the same or different size. Energy between cavities is coupled via slots of different shapes and positions.

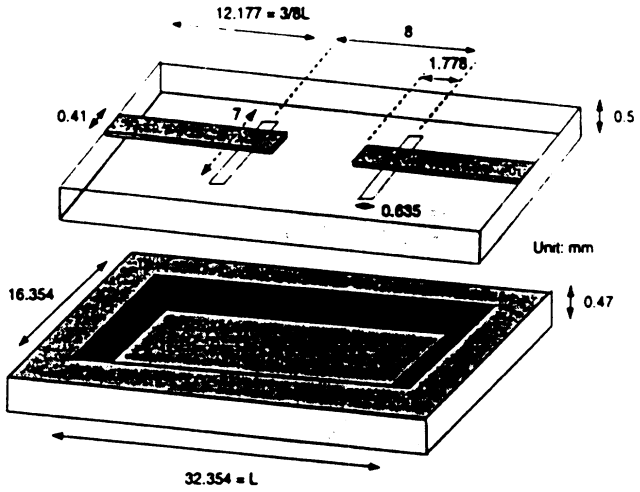

Figure 1: X-Band Resonator

Originally the slots are placed at 1/4 and 3/4 of the cavity length from the shorter edges of the cavity. Herein, we investigate both experimentally and theoretically the effects of reducing the distance between the two slots on the bandwidth and the insertion loss. In addition, theoretical results indicating the effect of

packaging on the performance of the resonator will be presented.

II Results and Discussion

The resonator shown in Fig.1 with the slots positioned at 3/8 and 5/8 of the cavity length from the shorter edges has been fabricated using two high resistivity 500 μm thick silicon wafers, with PECVD nitride grown on both sides of them. The microstrip lines are formed on the top surface of the first wafer by gold electroplating to a total thickness of 6 μm. CPW to microstrip transitions are included in order to measure the resonator with on-wafer probing. The ground planes of the CPW and microstrip lines are set at the same potential with the help of via holes. The cavity is fabricated on the second wafer by using chemical anisotropic etching (TMAH water based solution) up to a depth of 470 μm and is then metallized to a thickness of approximately 3 μm. The two wafers are finally bonded together using silver epoxy glue that is cured at $150°C$.

The fabricated resonator was measured using a TRL (Thru-Reflect-Line) calibration referenced at the slots and the results are compared with theoretical ones in Fig. 2. Theoretical results were obtained by using the HP High Frequency Structure Simulator [4]. As can be seen from Fig. 2 there is very good agreement between the simulated and measured response. The small discrepancy (1%) in the resonant frequency can be attributed to the inherent numerical error of the HFSS software and fabrication tolerances. The measured resonator exhibits a bandwidth of 2% (210 MHz) at a resonant frequency of 10.525 GHz. The insertion loss, after de-embedding the loss on the two open end stubs extending beyond the center of the slots, is measured to be -1.1 dB. Comparison of these results to the ones presented in [1] can be seen in Fig. 3 where we observe a 58% reduction in the bandwidth (from 500 to 210 MHz) and a 0.74 dB increase in insertion loss. These results indicate that by altering the positions of the coupling slots relative to the center of the cavity we can change (increase or decrease) the bandwidth of the resonator at the price of increased loss. This of course is expected since the

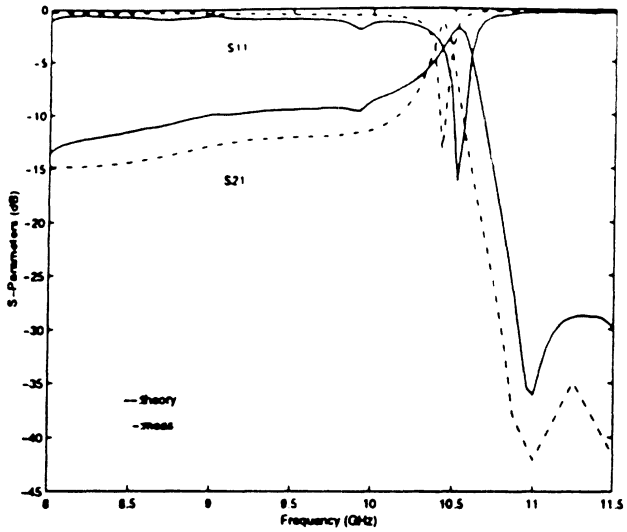

Figure 2: Measured and simulated results for the resonator of Fig.1.

Q_u of the resonator is determined by the cavity and is independent of the position of the slots. Preliminary simulations and measurements of the resonator with the slots positioned at 1/8 and 7/8 of the cavity length from the shorter edges show a bandwidth much greater than the original one of 500 MHz.

From Fig. 2 we can also observe a slight asymmetry in the response around the resonance. This is due to the fact that the two microstrip lines are close enough (0.4 λ_g) and power is coupled from one to the other directly via substrate modes. In order to eliminate this effect and make the response more symmetric around resonance we can use micromachined on-wafer packaging [5] to isolate the microstrip lines from one another both on top and inside the substrate. For this purpose an HFSS simulation was run where one PEC plane is placed on top of the structure and another is placed between the two lines shorting the top pec to the slot plane. Results can be seen in Fig. 4, where we observe that packaging reduces the suspected coupling occuring below 10.3 GHz by as much as 4 dB. In addition, we observe that there is a small coupling of about -16 dB below 10 GHz that can be attributed to evanescent modes excited around the slots inside the cavity. Presently study is under

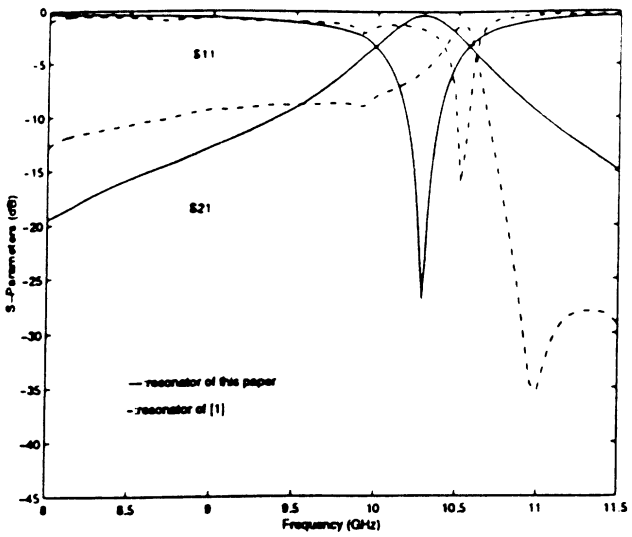

Figure 3: Measured results for the two resonators with different slot positions.

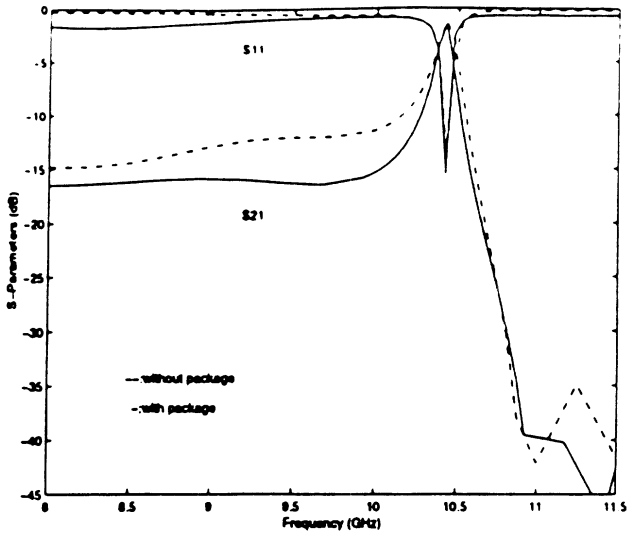

Figure 4: Simulated response of the packaged and non-packaged resonator.

way to further understand the effect of evanescent modes and improve out-of-band rejection. In a micromachined filter design with multiple cavities evanescent modes can be used instead of propagating ones to decrease the size of the cavities since these modes operate below cut-off.

III Conclusions

The effects of slot positions in a micromachined resonator have been presented. Although the Q_u is determined by the cavity itself, the bandwidth is determined by the relative position of the slots. Specifically when the slots are placed closer to the center of the cavity the bandwidth is reduced and the insertion loss is increased. The close proximity of the slots also produces direct coupling between the microstrip lines that can be eliminated with appropriate packaging of the structure and evanescent modes that affect the shape of the response around resonance.

IV Acknowledgement

This work was partly funded by the U.S. Army Research Office (MURI program) and partly by the U.S. Office of Naval Research.

References

[1] J. Papapolymerou, J.C. Cheng, J. East and L.P.B Katehi, "A micromachined high-Q X-Band resonator," *IEEE Microwave and Guided Wave Letters*, Vol. 7, No. 6, pp. 168-170, June 1997.

[2] R.F. Drayton, T.M. Weller and L.P.B. Katehi, "Development of miniaturized circuits for high-frequency applications using micromachining techniques," *International Journal Microcirc. Elec. Packaging*, vol. 3, 1995.

[3] R.E. Collin,*Foundations for Microwave Engineering*. New York: McGraw-hill, 1966, pp. 322-325.

[4] HP 85180A High-Frequency Structure Simulator User's Reference, Hewlett-Packard Company, 1994.

[5] R.F. Drayton, R.M. Henderson and Linda P.B. Katehi, "Monolithic packaging concepts for high isolation in circuits and antennas," *to be published in IEEE Transaction on Microwave Theory and Techniques.*

Appendix III

Low-Loss. Low-Activation Voltage Switches

Micromechanical Electrostatic K-Band Switches

Sergio Pacheco[1], Clark Nguyen[2] and Linda Katehi[1]
The Radiation Laboratory[1]
Center for Integrated Sensors and Circuits[2]
University of Michigan
Ann Arbor, MI 48109-2122

Outline

- Motivation
- Micromechanical Switch Design
- Fabrication Process
- DC & RF Characteristics
- Application: Stub Design
- Stub RF Measurements
- Conclusions

Motivation

- Electrostatic capacitive switching is ideal for low power systems such as wireless and/or space/airborne applications

- Compatibility of the fabrication process with MMIC and CMOS technology allows for faster integration and lower costs

Switch Design

Design Concept for Micromechanical Electrostatic Switch

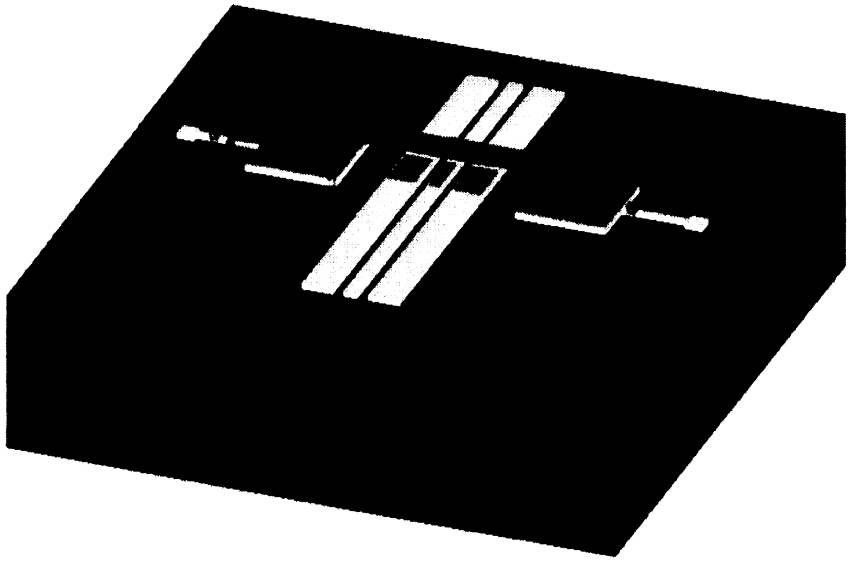

Pull-in Voltage:

K - spring constant

g_0 - gap

ε_0 - permittivity of air

A - actuation area

Switch Design

TOP VIEW

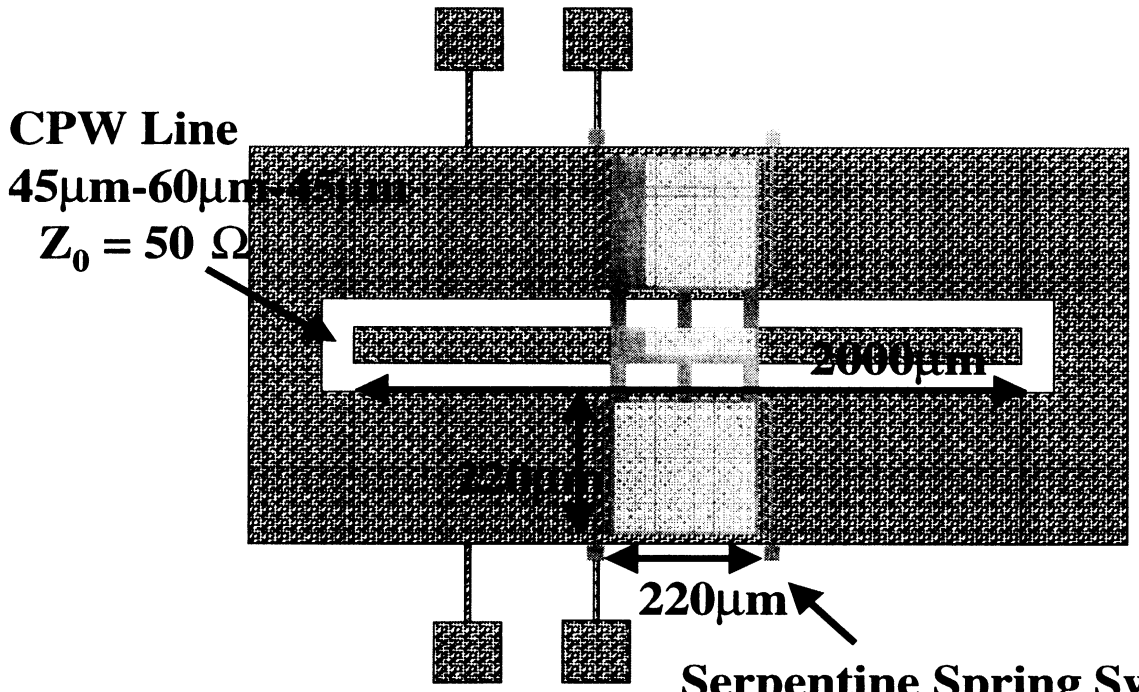

CROSS-SECTION

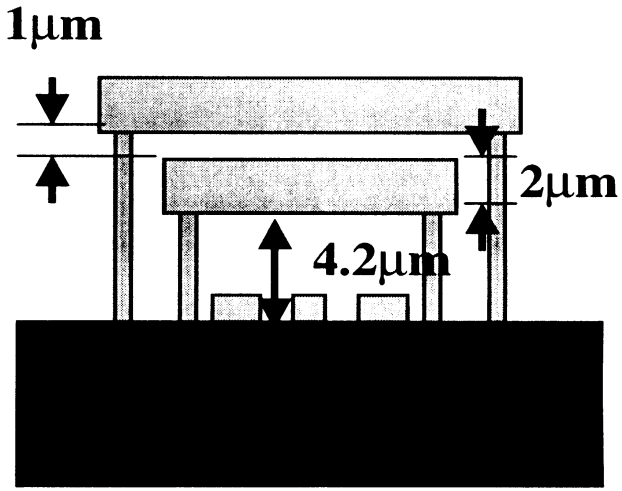

Circuit metal: 500/4500 Å
Ti/Au

Switch Design

Mechanical and Physical Parameters for Switches

	Serpentine	Cantilever
Spring Length	220 μ	250 μ
Spring Width	4 μ	4 μ
Number of Meanders	2	1
Gap	4.2 μ	4.2 μ
Actuation Plate Size	220 μ x 220 μ	220 μ x 220 μ
Mass	1.48×10^{-9} kg	1.49×10^{-9} kg
Spring Constant	0.478 N/m	0.654 N/m
Damping Coefficient	6.76×10^{-7} N/m/s	6.76×10^{-7} N/m/s
Actuation Voltage	4.95 V	5.79 V
Resonant Frequency	17.97 kHz	20.95 kHz

Switch SEM Photos

Serpentine Spring Design

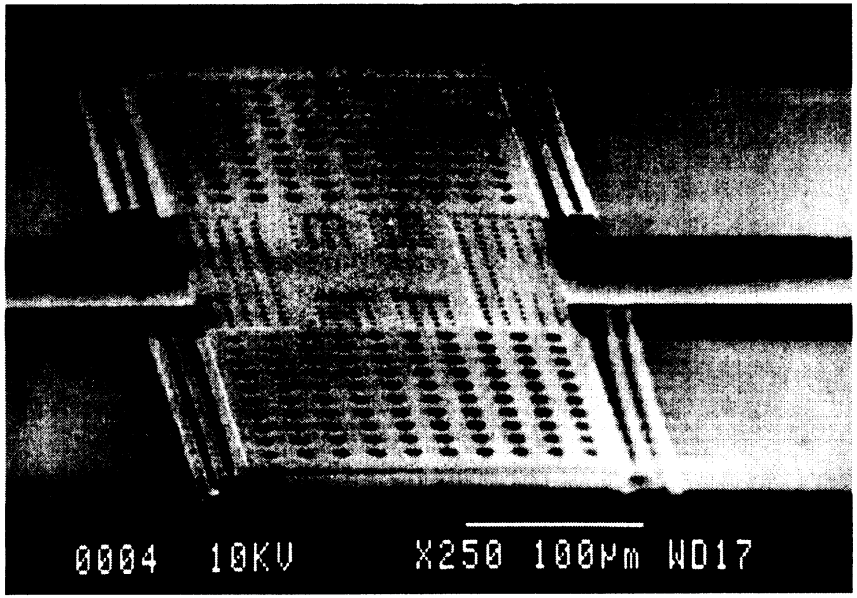

Cantilever Spring Design

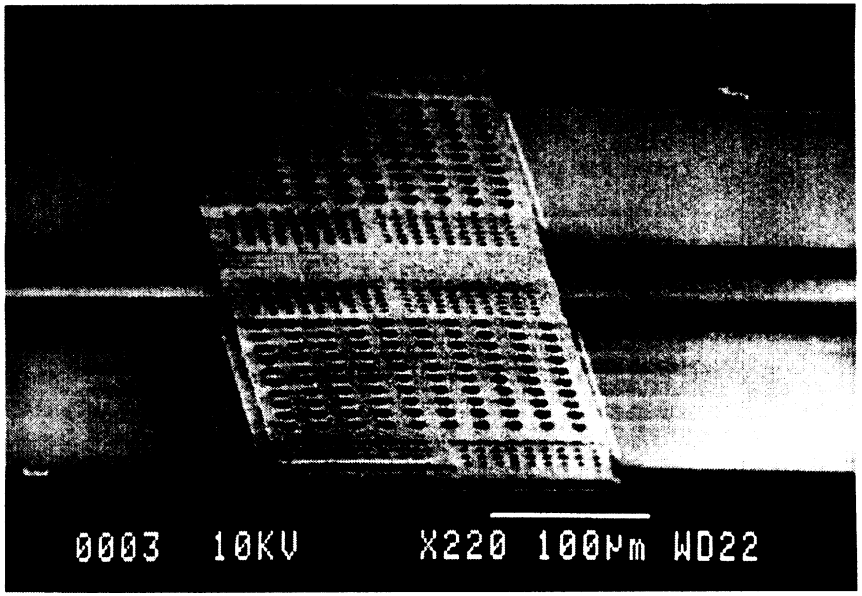

Fabrication Process

CIRCUIT METALIZATION

POLYIMIDE SACRIFICIAL LAYER 1
OPEN SWITCH ANCHOR POINTS

SWITCH BEAM DEFINITION AND METALIZATION

POLYIMIDE SACRIFICIAL LAYER 2
OPEN TOP ELECTRODE ANCHOR POINTS

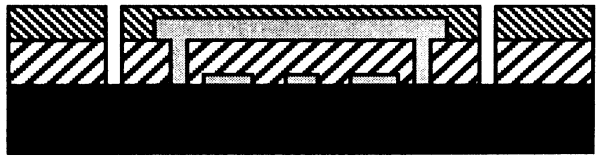

TOP ELECTRODE DEFINITION AND METALIZATION

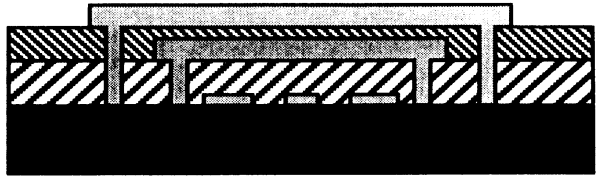

WET ETCH OF POLYIMIDE LAYERS AND SUPERCRITICAL CO_2 RELEASE

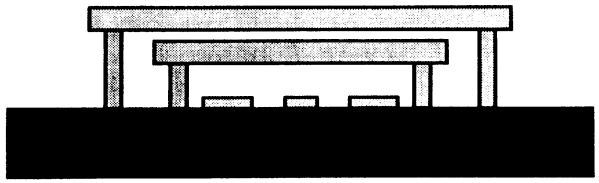

DC Measurements

Serpentine Spring Design

Cantilever Spring Design

Measurements performed with
an HP 4285A LCR meter at 100 kHz

DC Measurements

Serpentine Spring Design

Cantilever Spring Design

Measurements performed with
an HP 4285A LCR meter at 100 kHz

RF Measurements

Serpentine Spring Design

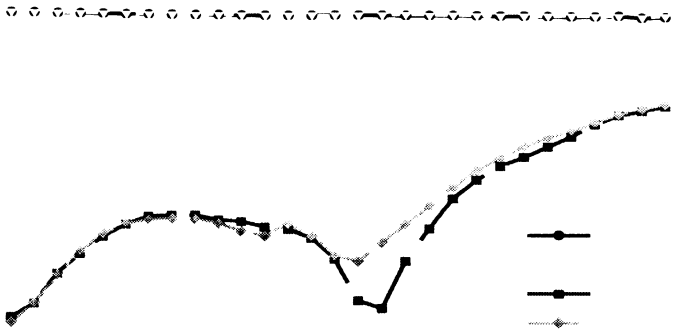

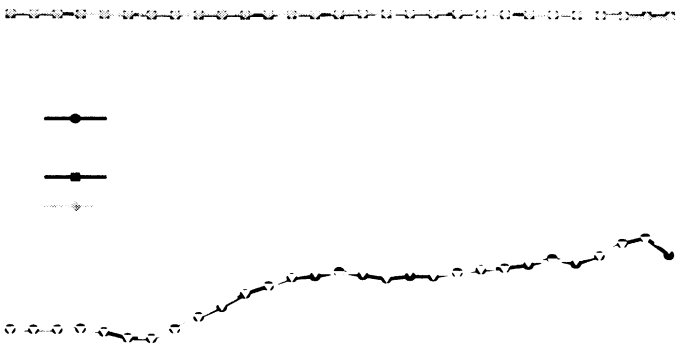

Measured on thru line 2mm long
Total loss: 0.26 dB
Attenuation: 0.13 dB/mm

RF Measurements

Serpentine Spring Design

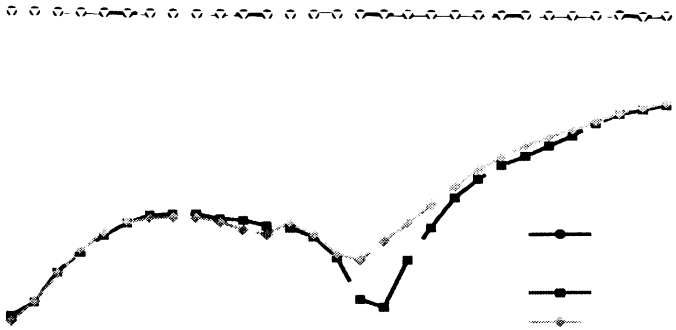

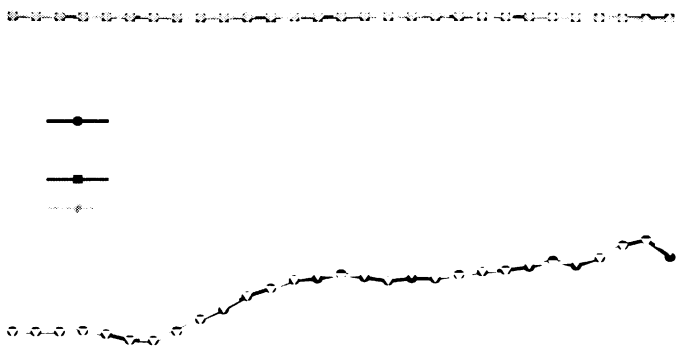

Measured on thru line 2mm long
Total loss: 0.26 dB
Attenuation: 0.13 dB/mm

RF Measurements

Cantilever Spring Design

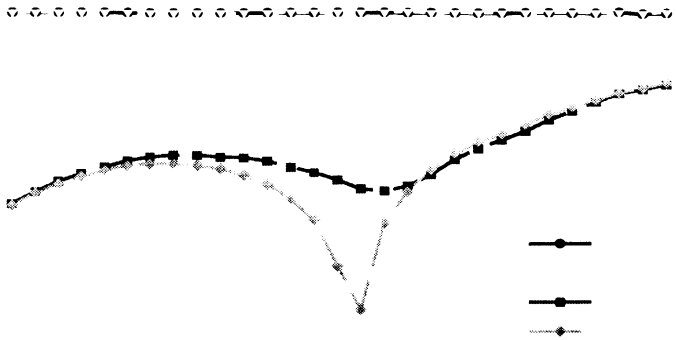

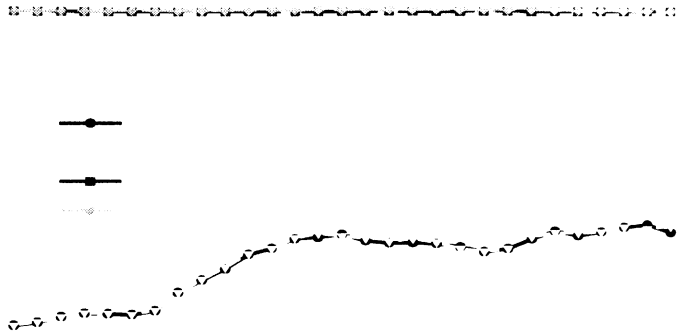

Measured on thru line 2mm long
Total loss: 0.28 dB
Attenuation: 0.14 dB/mm

RF Measurements

Cantilever Spring Design

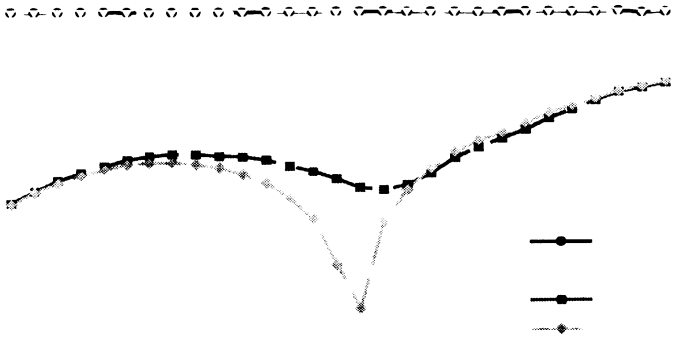

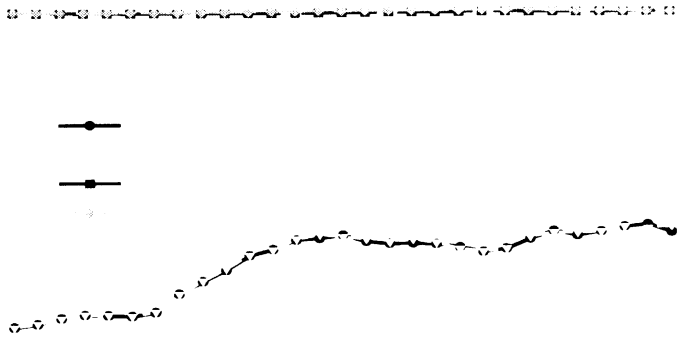

Measured on thru line 2mm long
Total loss: 0.28 dB
Attenuation: 0.14 dB/mm

Appendix VI

A Compact. High Isolation MEMS SPDT Switch with Low-Voltage Control

A Compact High Isolation MEMS SPDT Switch with Low-Voltage (6-12 V) Control

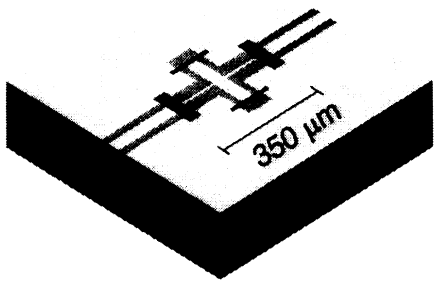

Prof. Gabriel M. Rebeiz
with
Jeremy B. Muldavin, Graduate Student

EECS Department
The University of Michigan*
Ann Arbor, MI 48109-2122
Tel: (734) 647-1793
Fax: (734) 647-2106
rebeiz@engin.umich.edu

Abstract

We propose the development of a novel compact high isolation MEMS-based switch. The switch is based on a novel design, developed at the University of Michigan, and can be controlled by a low pull-down voltage (6-12 V depending on the residual stress in the membrane switch layer). The total size of the MEMS chip is approximately 0.35x0.31mm on a silicon substrate and 0.57x0.50 mm on a quartz substrate. The insertion loss of the switch in the OFF position (bridges are up) is expected to be less than -0.8 dB (with an S_{11} below -20 dB). The isolation of the switch in the ON position (bridges are down) is expected to be lower than -50 dB over the frequency operation range. A SPDT design of this novel switch will also be implemented. Finally, accurate electromagnetic models of the switch will be developed. These models are essential in the future development of Single-Pole-Multiple-Throw switches.

I. Introduction

Several US companies [1-3] are currently developing MEMS (Micro-Electro-Mechanical-Systems) switches for low-loss microwave and mm-wave applications. The MEMS switches typically consist of a metal bridge (typically 0.5-1 μm of Au or Al) which is suspended 3-4 μm above a microwave transmission line. The switches are pulled down to the line using an electrostatic voltage (25-50 V) which depends on the residual stress and dimensions of the MEMS bridge. MEMS switches have shown some impressively low insertion at mm-wave frequencies, with a quoted value of -0.1 dB/10 GHz from 10-60 GHz.

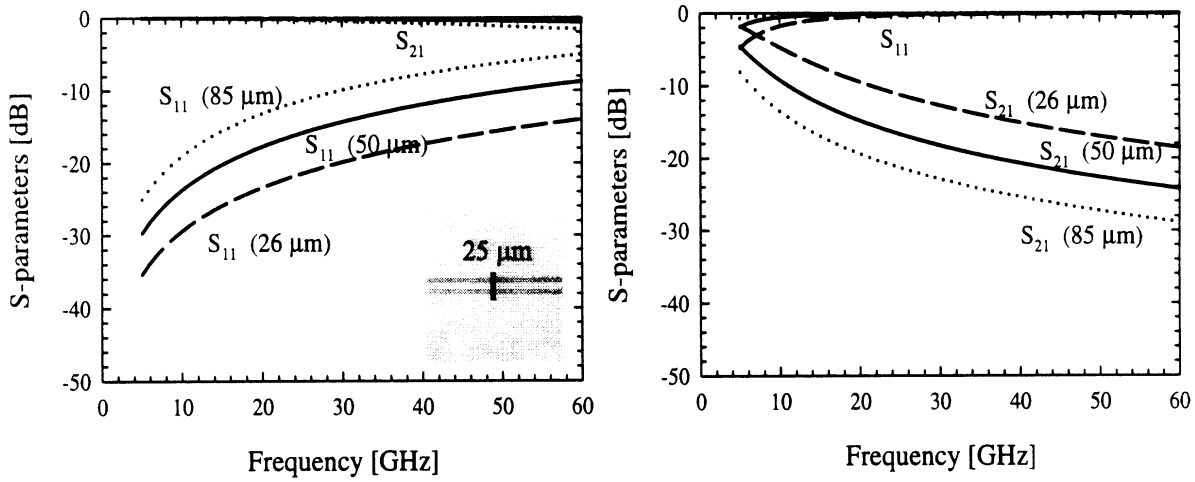

Figure 1 *The insertion loss and isolation of a single MEMS bridge with dimensions of 26 μm, 50 μm and 80 μm over a 100 μm-wide cpw-line on a silicon substrate, shown in the OFF and ON state from left to right. The MEMS bridges are 1.5 μm high resulting in OFF state capacitance values of 15.3, 29.5, 47.2 fF, respectively. The ON state capacitance is 0.92, 1.78, 2.8 pF, respectively, with 1000 Å of a silicon nitride layer between the top metal bridge and the cpw-line.*

The isolation of MEMS switches at 30 GHz depends on the area of the bridge (and thus the capacitor value). If the bridge is too wide, resulting in a large ON and OFF-state capacitance, the switch will have good isolation (-23 dB) when switched ON (bridge is pulled down). However, in this case, the OFF-state performance of the switch suffers from a large reflection coefficient due to the somewhat large parasitic capacitance shunting the line (S_{11} may be as high as -10 dB). One way to solve this problem is to use two MEMS bridges spaced approximately 90° (λ/4) apart. The reflection from both bridges in the OFF-state cancel, and results in an excellent return

loss (S_{11} is around -20 dB over a 150% bandwidth). Also, when the bridges are switched ON, the insertion loss is that of two switches in series and can be as low as -30 to -40 dB.

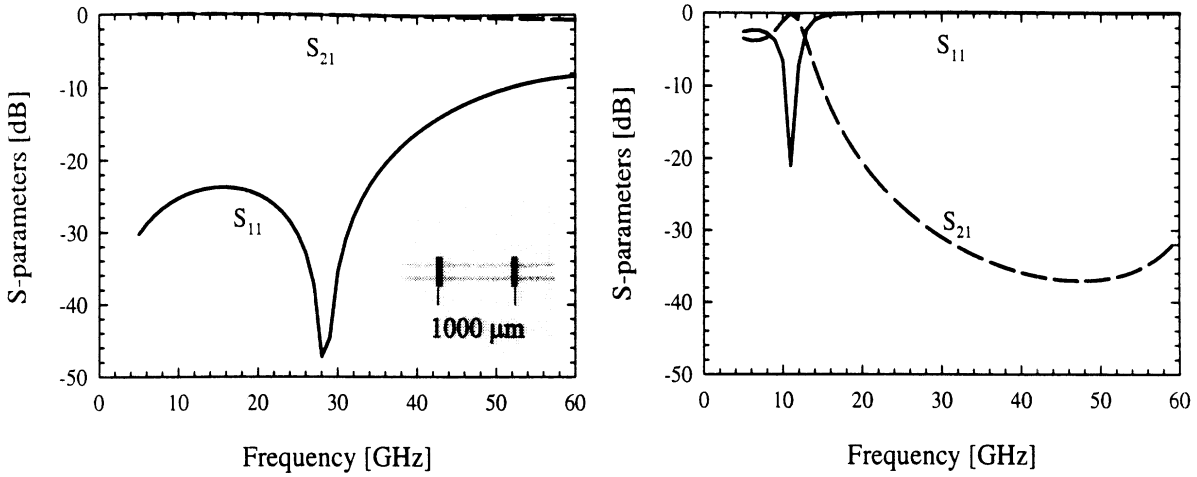

Figure 2 *The insertion loss and isolation of a double MEMS bridge with dimensions of 26 µm, over a 100 µm wide cpw-line on a silicon substrate (C_{off}= 15.3 fF, C_{on}= 0.92 pF, per bridge), shown in the OFF and ON state from left to right. The midsection line is 80 degrees long at 30 GHz. More isolation can be obtained with the use of larger MEMS bridges (up to -40 dB).*

II. The Novel Cross Switch

A novel design developed at the University of Michigan is the Cross-Swich (X-switch), shown in Figure 4. The cross switch consists of two in-line MEMS bridges (C_1= C_2 = 59 fF) for a low-reflection design with the addition of two short stubs loaded with two MEMS bridges (C_3= C_4 = 17.7 fF). The operation of the cross-switch is as follows: When the MEMS switch is in the OFF-state (bridges are up), the short stubs are open-circuited (actually loaded by a small parasitic capacitance, C3, in the UP-position) and therefore, appear as an open circuit at the cross-junction. There are many optimization parameters, such as the exact length of the cross lines, the line impedance and length between MEMS bridges C1 and C2, etc. It is quite possible to design a cross switch with an S_{11} of around -20 dB and an insertion loss of -0.6 dB. However, when the switch are in the ON-state (bridges are down), the short stubs are short-circuited and therefore appear as a short at the cross junction. This will result in a large reflection coefficient and therefore a very high isolation. A first design of the cross switch at 30 GHz is shown in Figure 4. The cross switch utilizes two in-line 100 µm wide MEMS bridges, and two 30 µm wide MEMS bridges at the end of the short stubs. The calculated isolation in the ON-state is more than -70 dB, while keeping an OFF-state reflection coefficient better than -20 dB over a 10 GHz bandwidth at 30 GHz. The total switch dimensions are around 900x800 µm, which is very small at 30 GHz. The expected cross-switch dimensions at 60 and 77 GHz are 450x400 µm and 350x310 µm, respectively.

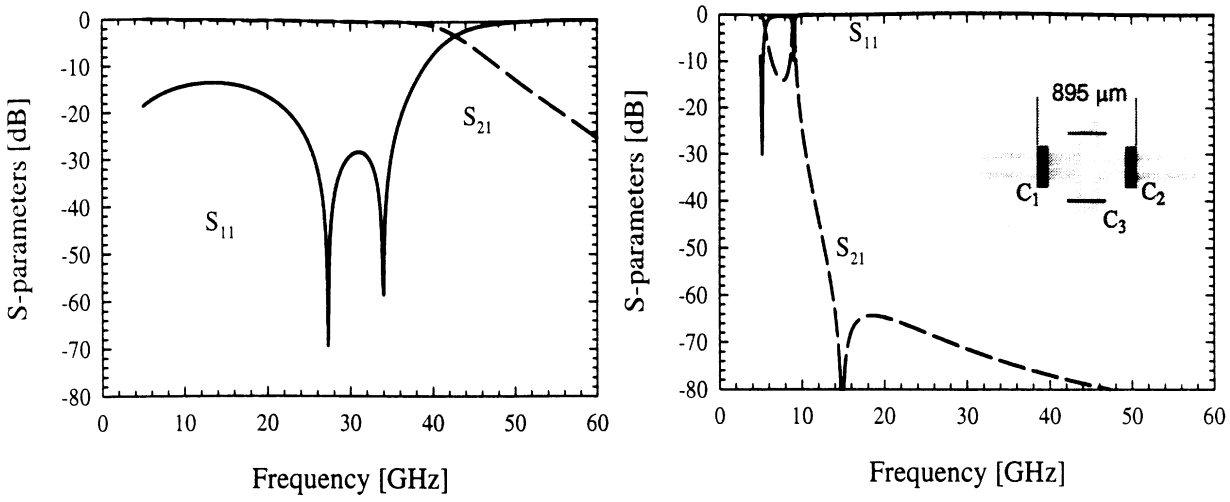

Figure 3. *The geometry of the cross-switch and its electrical performance, shown in the OFF and ON state from left to right. The same MEMS bridge parameters (height, nitride thickness, cpw line dimensions outside the MEMS cross switch, etc.) as Figs. 1 and 2 have been used. Only the MEMS bridge width is changed for this design.*

The cross switch results in excellent ON-state isolation (-70 dB or better) with minimal OFF-state insertion loss (-0.5 dB) at 60 GHz or 77 GHz. Figure 4 shows that an isolation of -70 dB can also be achieved by cascading several two-bridge designs at the expense of higher insertion loss (-2 to -3 dB) and much larger area on the MMIC wafer (around 3 mm x 200 µm at 30 GHz). Therefore, applications requiring around 10 GHz of bandwidth at 60 GHz or 77 GHz, the cross-switch is an excellent design offering very low insertion loss, extremely high isolation and occupying the least known amount of area on a chip.

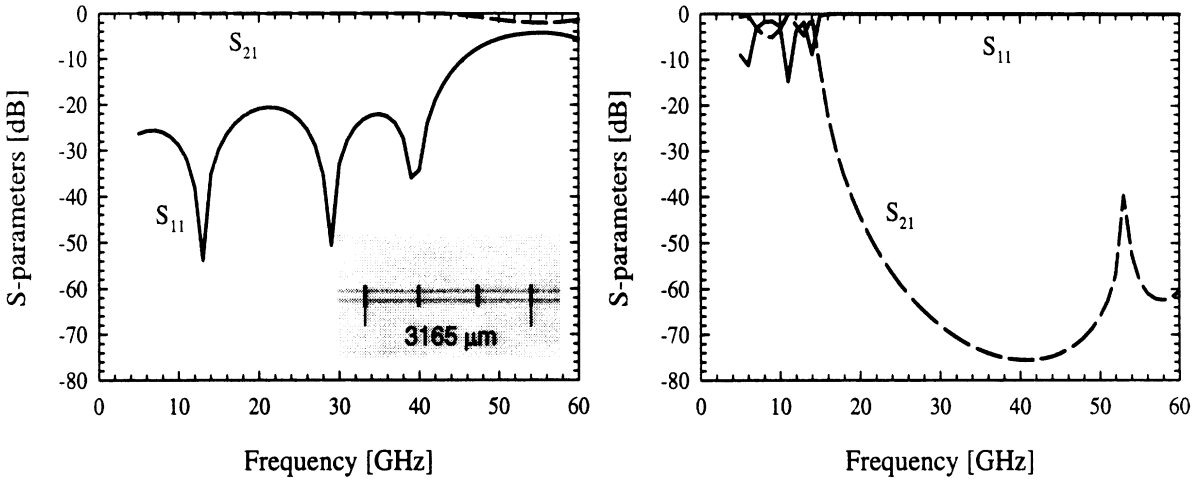

Figure 4. *The insertion loss and isolation of a cascaded double MEMS bridge with dimensions of 26 µm, over a 100µm wide cpw-line on a silicon substrate (C_{off}= 15.3 fF, C_{on}= 0.92 pF), shown in the OFF and ON state from left to right. The individual double MEMS bridge desings are as in Fig. 2. The midsection line is 105 degrees long at 30 GHz. More isolation can be obtained with the use of larger MEMS bridges.*

Once a cross-switch is designed successfully, we propose the implementation of a SPDT switch based on the same concept. In this case, a simple λ/4 line is used at the reactive T-junction of the SPDT switch. This ensures that an open-circuit appears at the T-junction in the port of the on-state switch (bridges are down), and therefore the incident power is all transferred to the line

with a switch in the off-state position. This is a standard design and is commonly used in all PIN diode SPDT switches. The SPDT switch will be fabricated and measured at 77 GHz for automotive applications.

III. Bridge Height vs. Pull-down Voltage

Typical MEMS switches today are built with bridge heights of 3-4 μm which results in a low parasitic capacitance when the bridges are up (off state). However, in two-bridge designs, this parasitic capacitance is tuned with the use of the 90-degree line between the bridges and therefore is not important in the designs. We propose the use of a bridge height of 1.5 μm instead of 3 - 4 μm resulting in a lower actuation voltage (6-10 V instead of 28-50 V). Also, the MEMS bridge has to move 1.5 μm instead of 3.5 μm and therefore is about twice as fast (1-2 μsec compared to 2-4 μsec for the same design but with a bridge height of 3-4 μm). The disadvantage is that the switch will suffer from hot-RF switching effects at lower RF powers, around 2-3 W instead of 4-6 W for the 3-4 um bridge height.

IV. RF MEMS Bridge Modeling

The research effort will also concentrate on the development of an electromagnetic model of the RF-MEMS bridge based on the physical aspects of the bridge (bridge height, width, length, thickness, and conductivity). Several bridges with varying width, length, and height will be fabricated and measured from 0-60 GHz and 70-110 GHz. This data will be used, together with an electromagnetic/physical model, to determine an equivalent circuit of the bridge with the physical parameters embedded in the electrical circuit elements (capacitance, inductance, and resistance). We believe that this model will result in a much faster design cycles of MEMS switches, especially those employing several bridges for SPMT designs.

References

[1] Goldsmith, C., J. Randall, S. Eshelman, T.H. Lin, D. Denniston, S. Chen, B. Norvell, "Characteristics of Micromachined Switches at Microwave Frequencies," *1996 IEEE MTT-S Intl. Microwave Symp. Dig.*, San Francisco, CA, June 17-21, 1996, pp. 1141-1144.

[2] Yao, J. J. and M. F. Chang, "A Surface Micromachined Miniature Switch for Telecommunications Applications with Signal Frequencies From DC up to 4 GHz," *Int. Conf. On Solid-State Sensors and Acutators Dig.*, Stockholm, Sweden, June 25-29, 1996, pp. 384-387.

[3] Larson, L. E., R. H. Hackett, M. A. Melendes, R. F. Lohr, "Micromachined Microwave Actuator (MIMAC) Technology – A New Tuning Approach for Microwave Integrated Circuits," *1991Microwave and Millimeter-Wave Monolithic Circuits Symp. Dig.*, Boston, MA, June 10-14, 1996, pp. 27-30.

Appendix V

SiGe/Si Microwave Amplifier Circuits

K-band Si/SiGe HBT MMIC Amplifiers using Lumped Passive Components with a Micromachined Structure

Liang-Hung Lu, Jae-Sung Rieh, Pallab Bhattacharya and Linda P.B. Katehi
Department of Electrical Engineering and Computer Science
University of Michigan, Ann Arbor, MI 48109-2122

E.T. Croke
Hughes Research Laboratory, 3011 Malibu Canyon Road, Malibu, CA 90265

George E. Ponchak and Samuel A. Alterovitz
NASA Lewis Research Center, Cleveland, OH 44135

Radiation Laboratory
The University of Michigan

OUTLINE:

- Motivation
- Si/SiGe HBTs
- Passive Components
- Process Integration
- Amplifier Design
- Summary

Motivation:

- Availability of Si/SiGe HBTs with advanced RF characteristics
- Lower cost compared with III V-based MMIC
- Compatibility with mature Si technology
- Mechanical stability of Si substrate
- Superior thermal conductivity of Si substrate

Si/SiGe HBTs

- **Epitaxial Layer Structure**

n+ Si	emitter contact	2×10^{19} cm^{-3}	2000 Å
n Si	emitter	2×10^{18} cm^{-3}	1000 Å
i $Si_{0.6}Ge_{0.4}$			50 Å
p+ $Si_{0.6}Ge_{0.4}$	base	2×10^{19} cm^{-3}	200 Å
i $Si_{0.6}Ge_{0.4}$			50 Å
n- Si	collector	5×10^{15} cm^{-3}	3000 Å
n+ Si	sub-collector	1×10^{19} cm^{-3}	15000 Å
p- Si	substrate	1×10^{12} cm^{-3}	540 μm

- **Photomicrograph of Fabricated HBT**

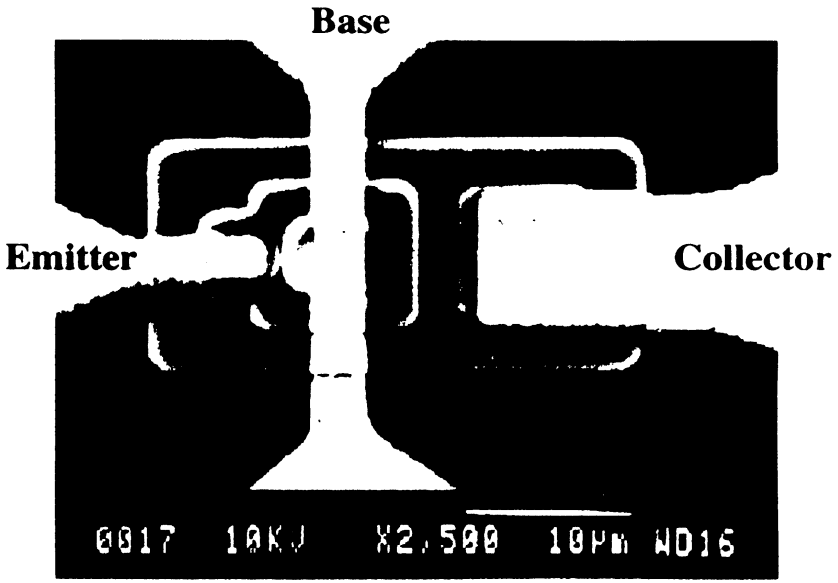

Radiation Laboratory
The University of Michigan

Si/SiGe HBTs (Cont'd)

- **I-V Characteristics**

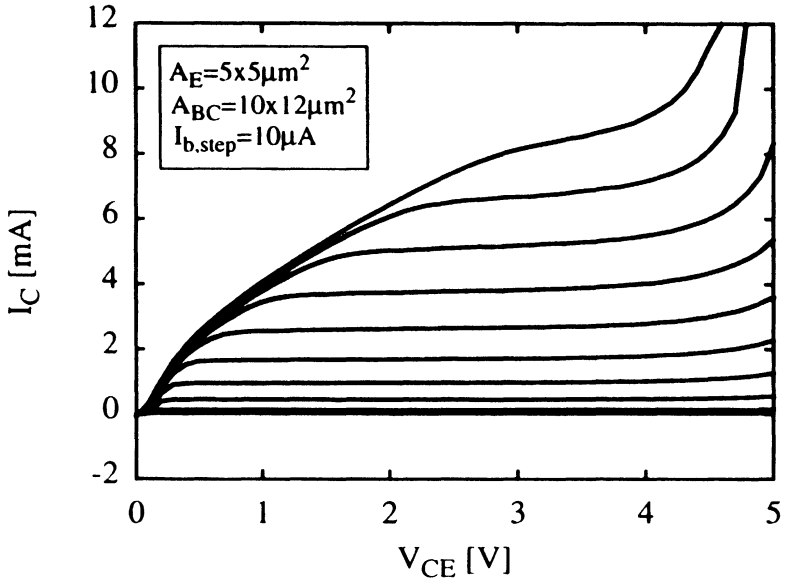

- **Gummel Plot**

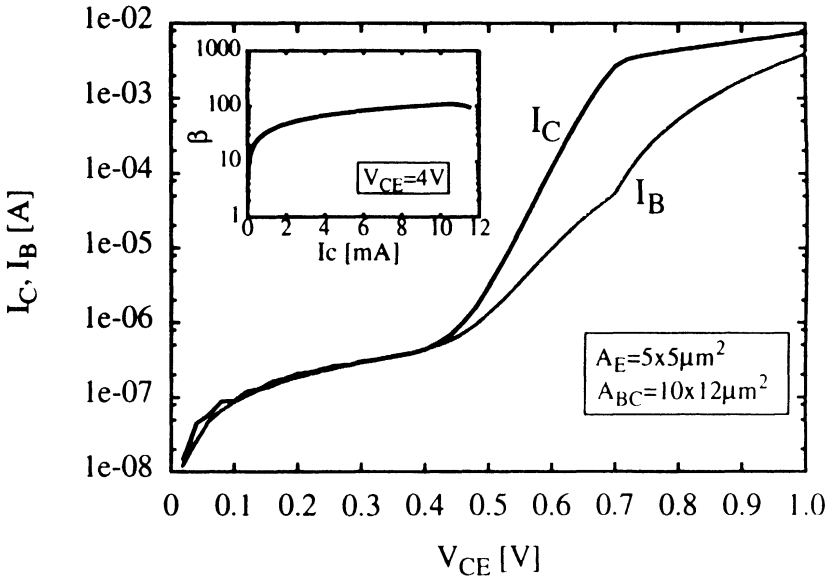

Radiation Laboratory
The University of Michigan

Si/SiGe HBTs (Cont'd)

- **Frequency Response**

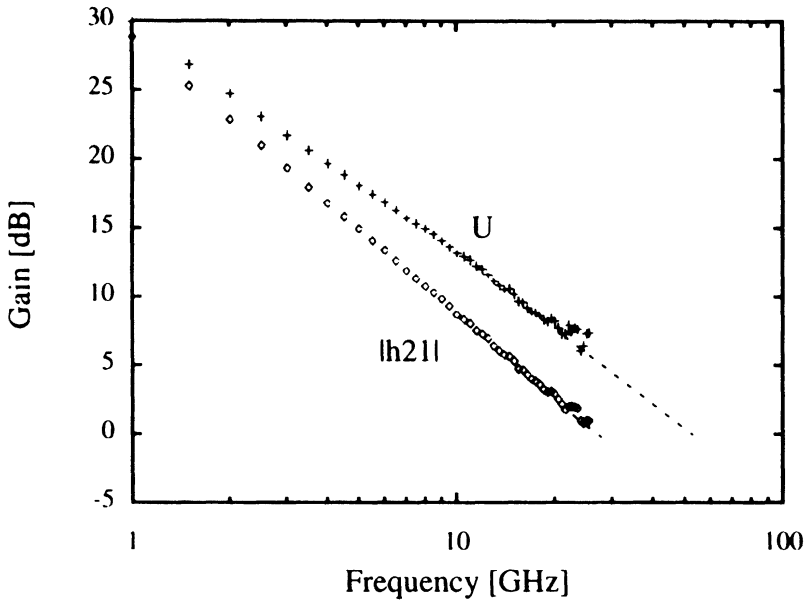

- **Bias Dependency of f_{max}**

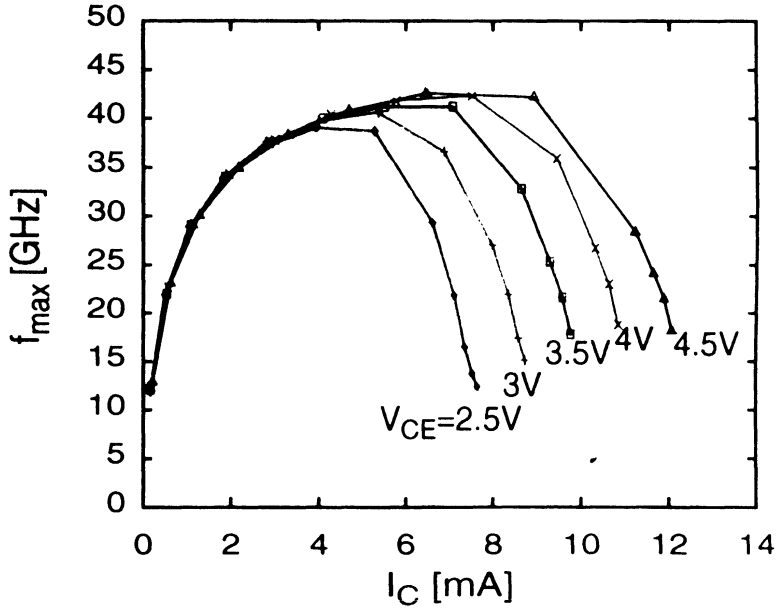

Radiation Laboratory
The University of Michigan

Si/SiGe HBTs (Cont'd)

- **Small Signal Equivalent Circuit and Parameters**

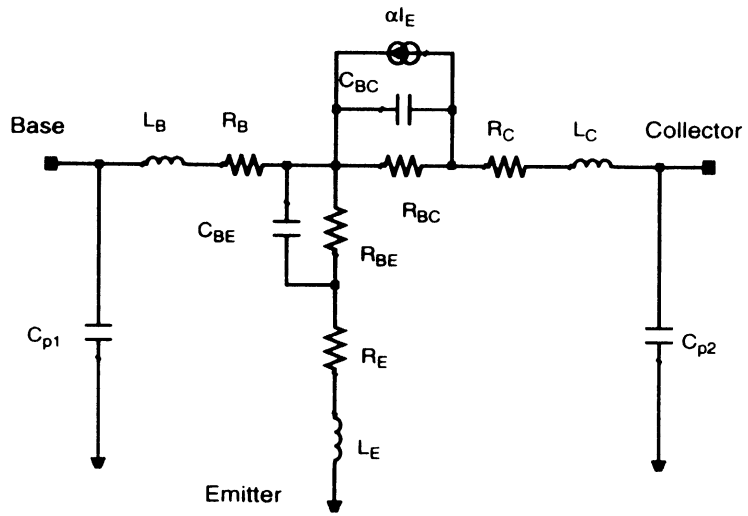

R_B	13.1 Ω	R_{BC}	127.0 kΩ
L_B	62.6 pH	C_{BC}	28.9 fF
R_{BE}	1.0 Ω	R_C	24.8 Ω
C_{BE}	106.8 fF	L_C	66.1 pH
R_E	15.8 Ω	$C_{p1,2}$	4.0 fF
L_E	141.7 pH	α_o	- 0.995

Passive Components

- Lumped components:
  - Thin-film resistors
  - Metal-insulator-metal capacitors
  - Micromachined spiral inductors
- Consideration:
  - Resonant frequency
  - Quality factors
  - Distributed effect

Thin-Film Resistors

- **Photomicrograph of the Thin Film Resistor**

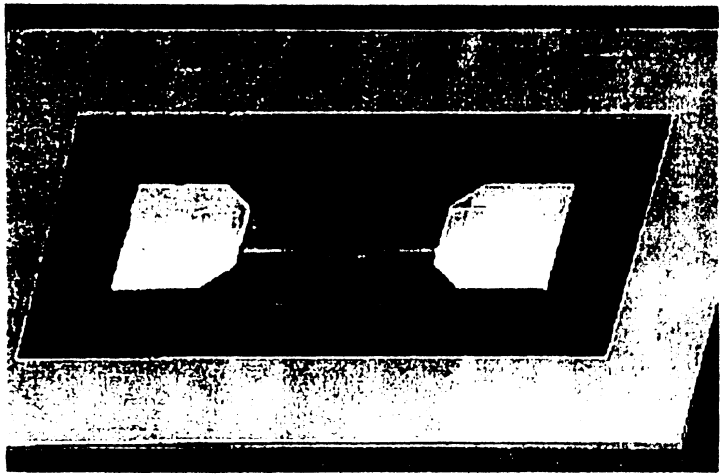

- **Small Signal Equivalent Circuits**

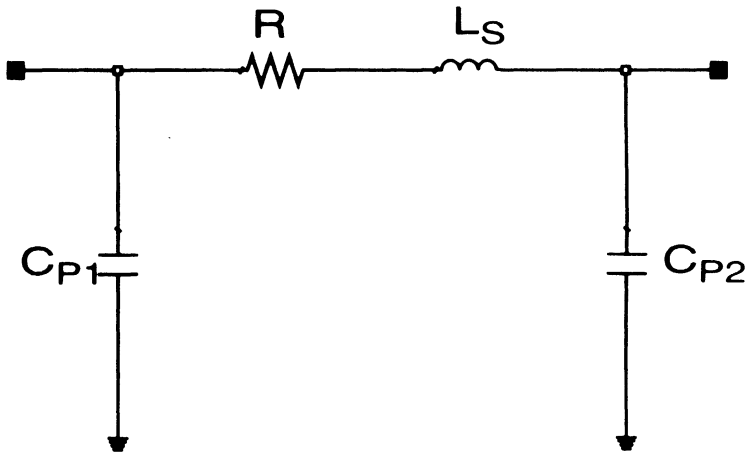

Sheet Resistance : 25~30 Ω (for a NiCr layer of 700Å)

MIM Capacitors

- **Photomicrograph of the MIM Capacitor**

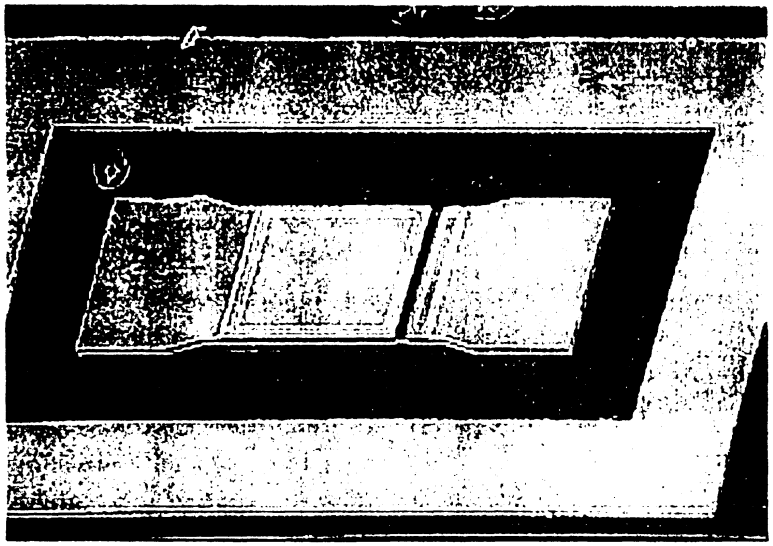

- **Small Signal Equivalent Circuit**

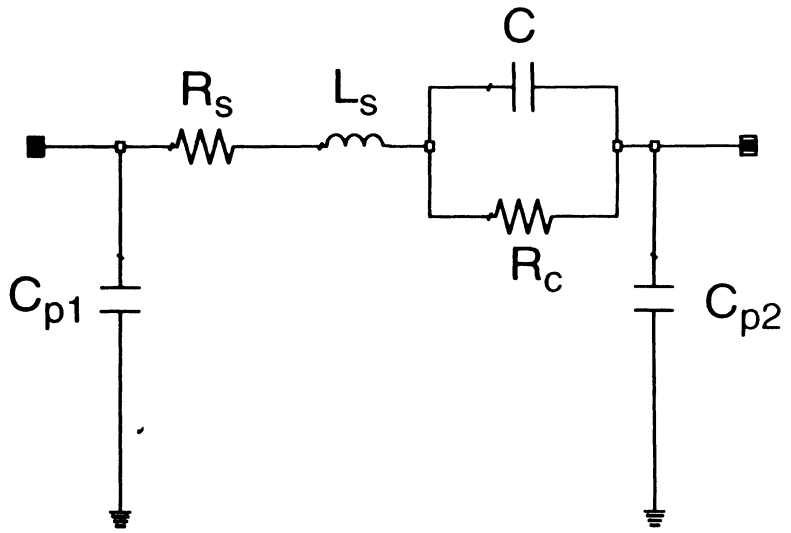

MIM Capacitors (Cont'd)

- **Summary of Performance Parameters**

Area (μm^2)	C (pF)	Q_{max}	f_{res} (GHz)
170	0.061	72.2	>40
340	0.110	70.5	>40
850	0.240	74.2	>40
1700	0.480	63.9	32.1
2550	0.780	57.2	23.5

- **Measured Quality Factors for the Capacitors**

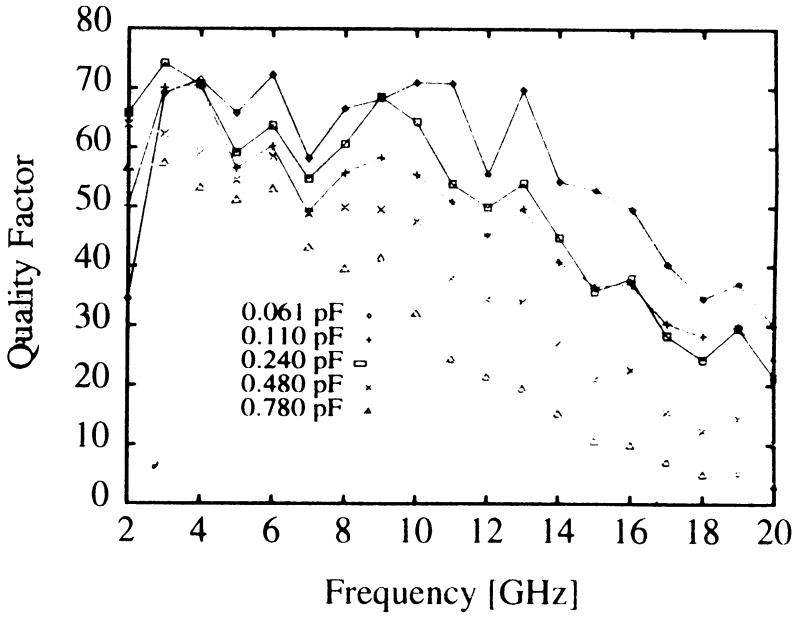

Micromachined Spiral Inductors

- **Frequency Response**

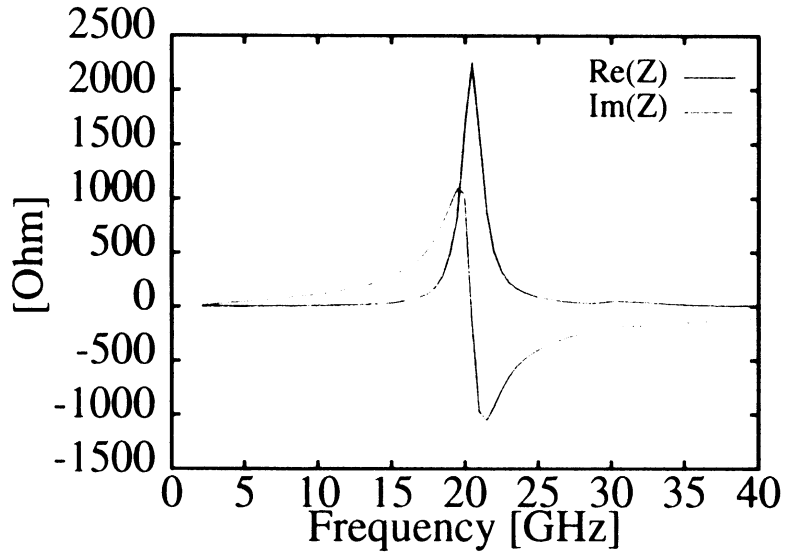

- **Small Signal Equivalent Circuit**

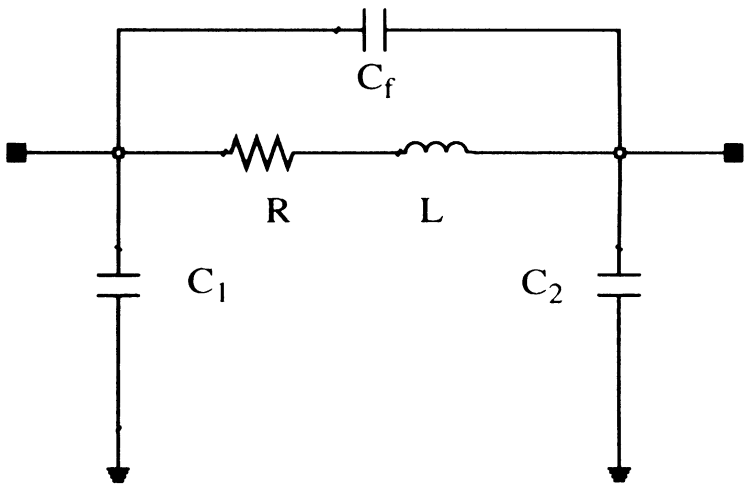

Micromachined Spiral Inductors (Cont'd)

- **Photomicrograph of the Micromachined Spiral Inductor**

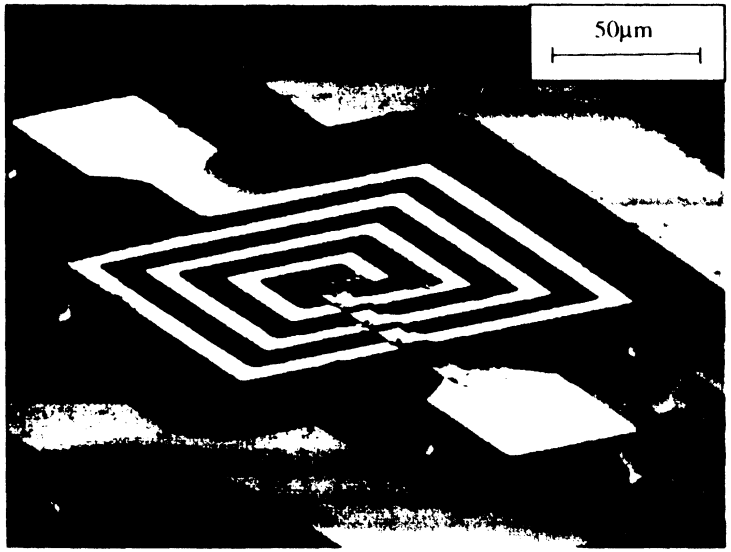

- **Summary of Performance Parameters**

For Etch Depth = 20 μm

Turns	L (nH)	Q_{max}/f_{Qmax} (GHz)	f_{res} (GHz)
1	0.17	12.1/40.0	>40
2	0.40	11.6/32.0	>40
3	0.88	11.4/19.2	>40
4	1.84	10.7/15.1	34.3
5	3.86	9.3/ 9.1	24.1
6	5.28	8.8/ 6.3	17.8

Micromachined Spiral Inductors (Cont'd)

- **Resonant Frequencies of Inductors with Various Etch Depth, d_{etch}**

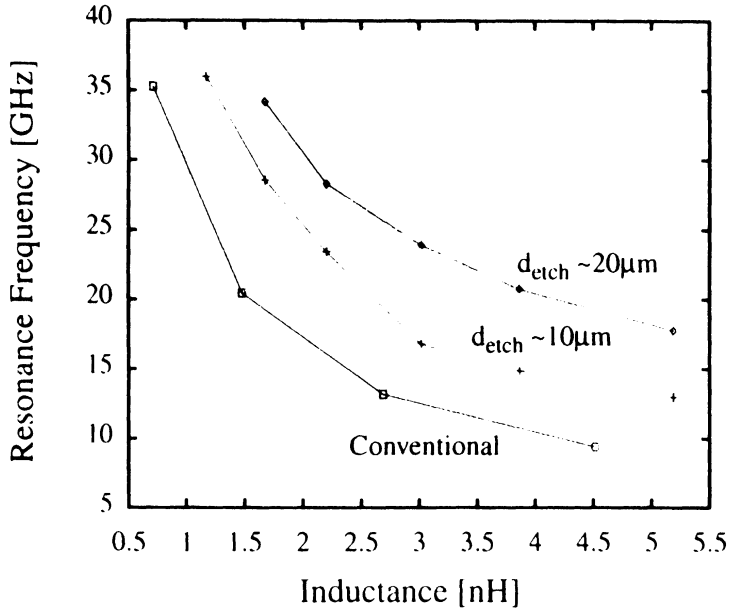

- **Measured Quality Factors for the Inductors**

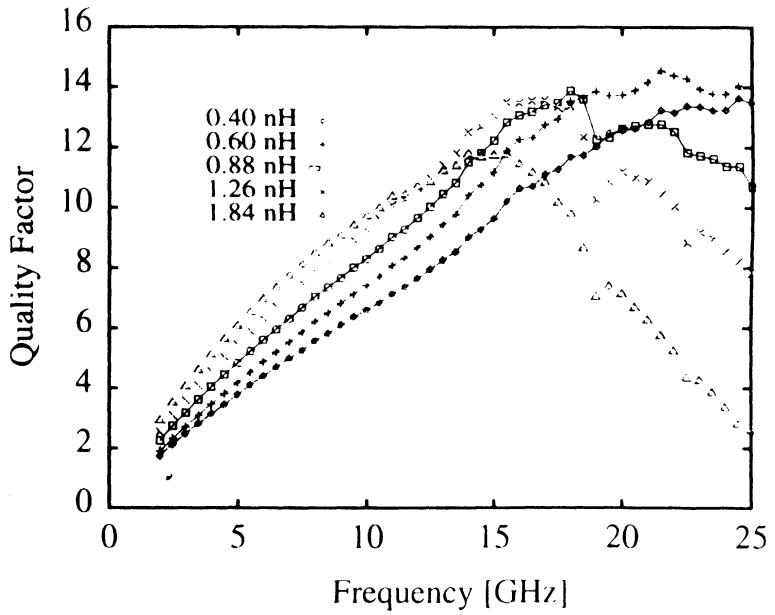

Radiation Laboratory
The University of Michigan

Process Integration

1. Emitter Metal and Emitter Mesa

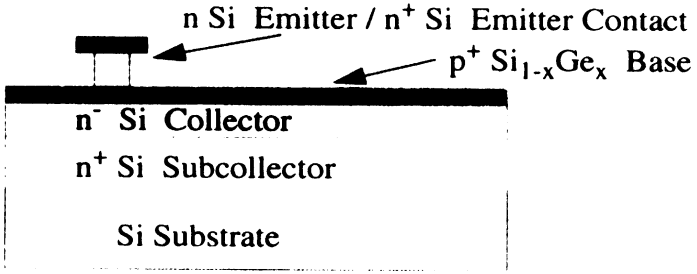

2. Base Metal and Base Mesa

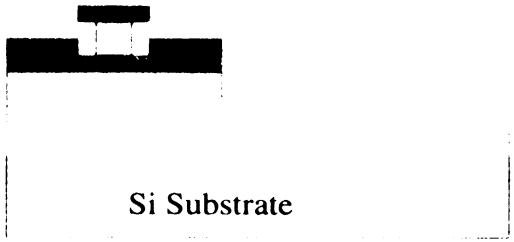

3. Collector Metal and Isolation

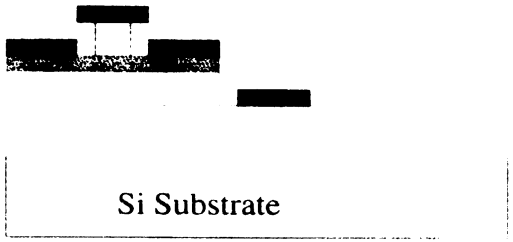

4. SiO_2 Dielectric Layer

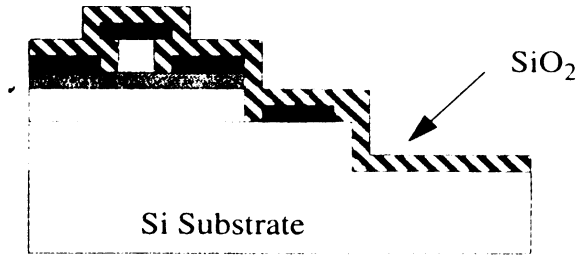

Process Integration (Cont'd)

5. Metal-Insulator-Metal Structure

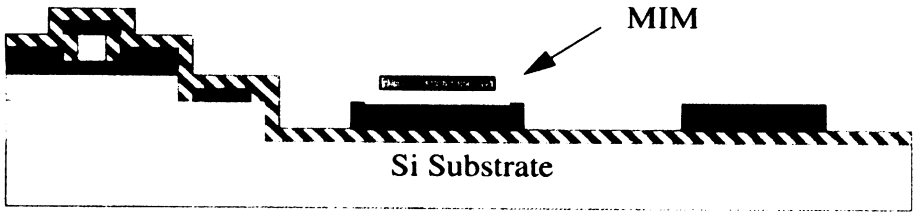

6. SiO_2 Passivation and Via Opening

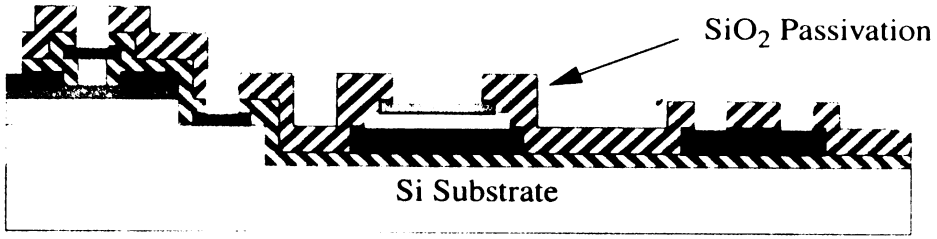

Process Integration (Cont'd)

7. Thin-Film Resistors and Interconnection

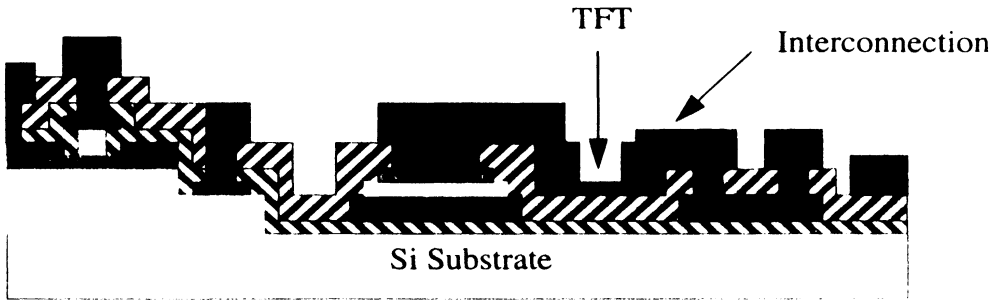

8. Deep RIE for Micromachined Structure

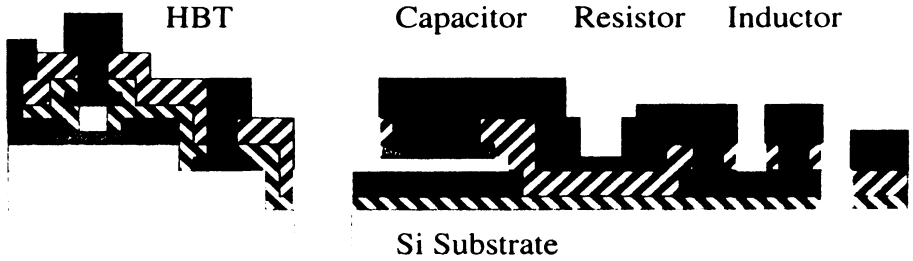

Amplifier Design

- **Schematic of the Single-Stage Amplifier**

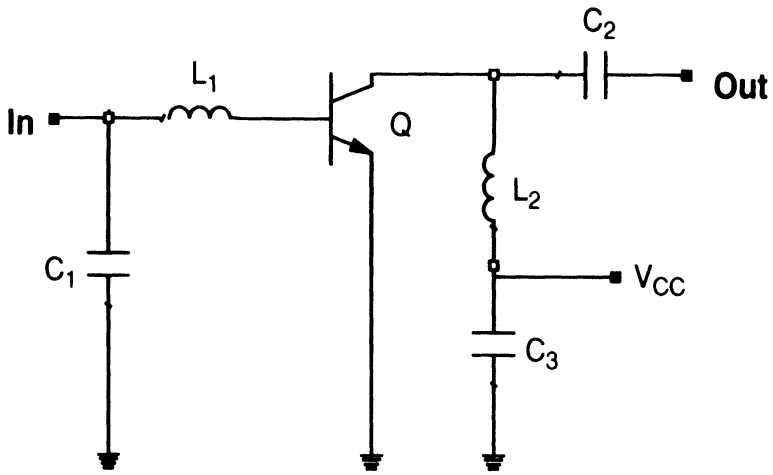

- **Photomicrograph of the Single-Stage Amplifier**

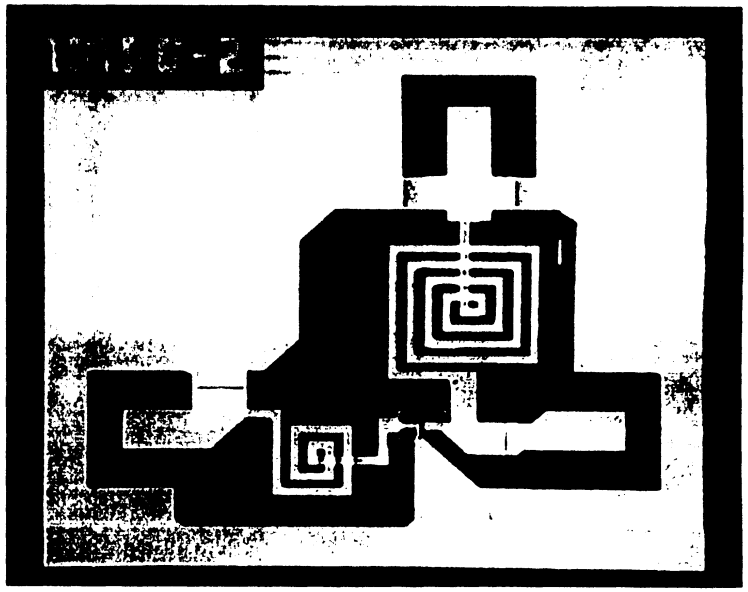

Amplifier Design (Cont'd)

- **Performance of the Single-Stage Amplifier (10 GHz)**

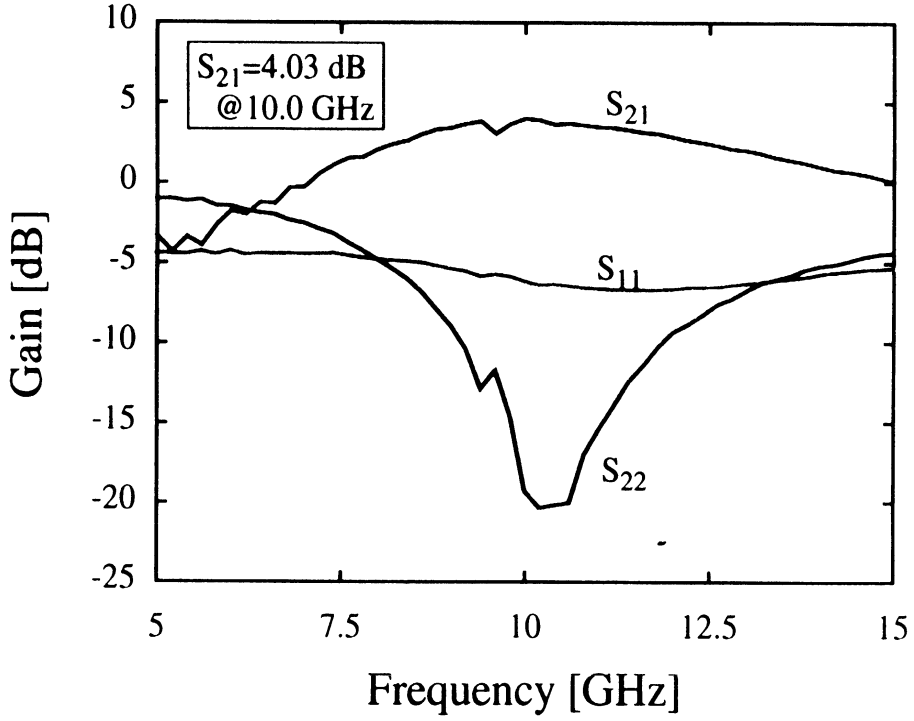

Amplifier Design (Cont'd)

- **Schematic of the Dual-Stage Amplifier**

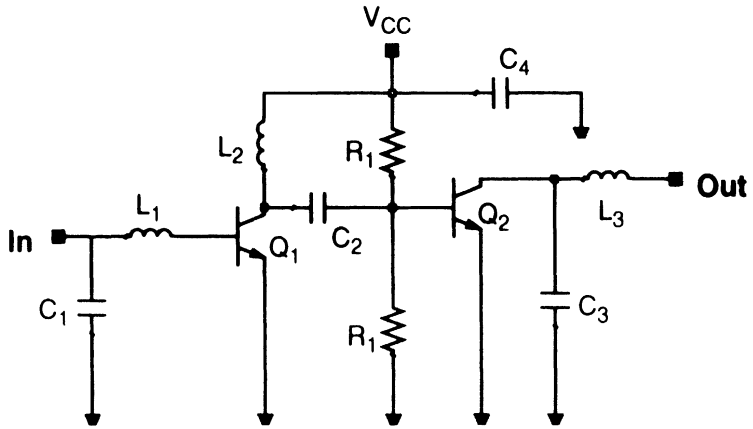

- **Photomicrograph of the Dual-Stage Amplifier**

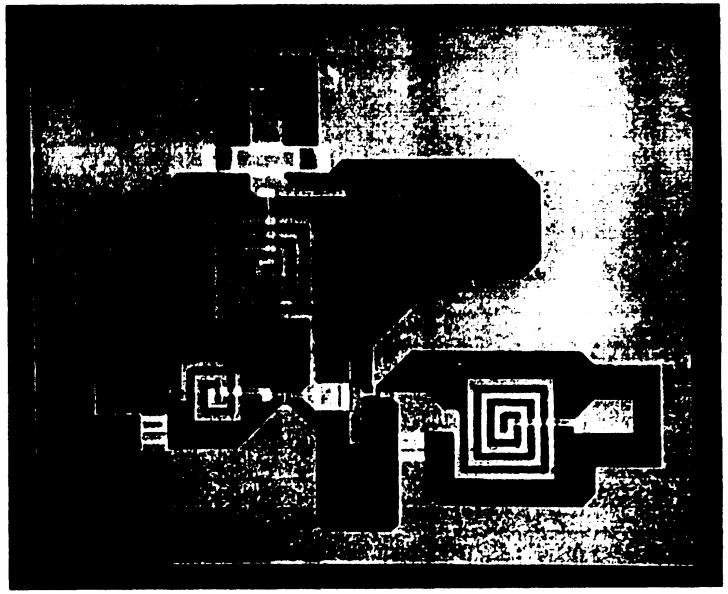

Amplifier Design (Cont'd)

- **Performance of the Dual-Stage Amplifier (10 GHz)**

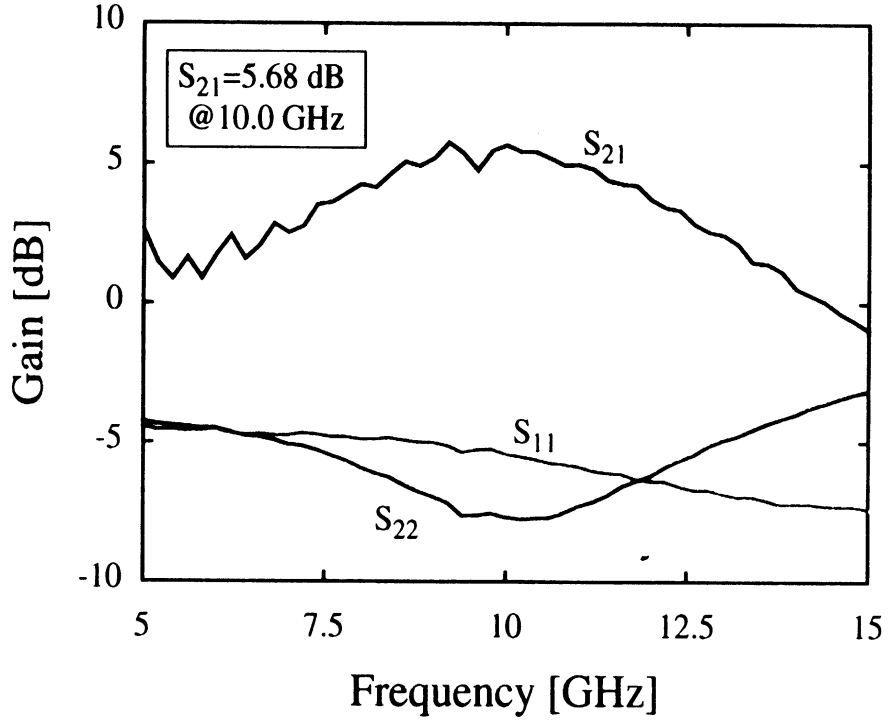

Amplifier Design (Cont'd)

- **Schematic of the Three-Stage Amplifier**

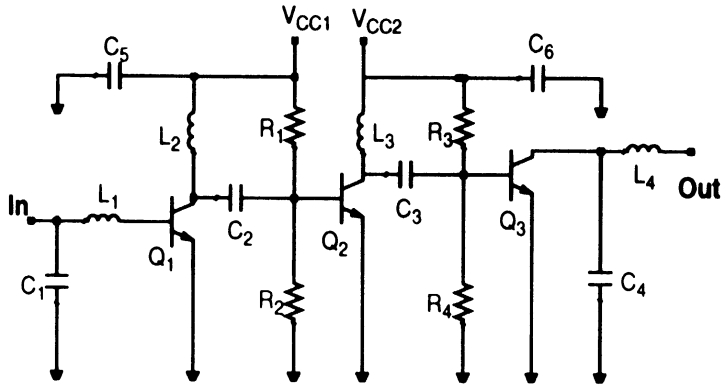

- **Photomicrograph of the Three-Stage Amplifier**

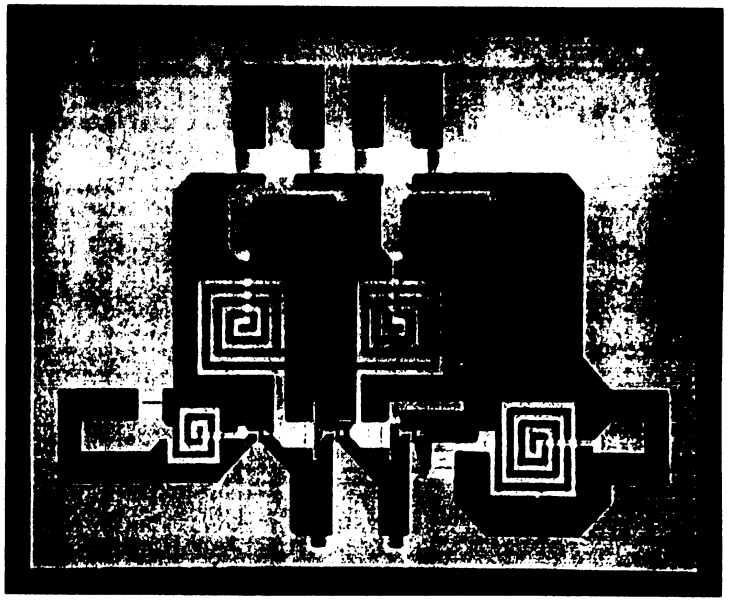

Amplifier Design (Cont'd)

- **Performance of the Three-Stage Amplifier (10 GHz)**

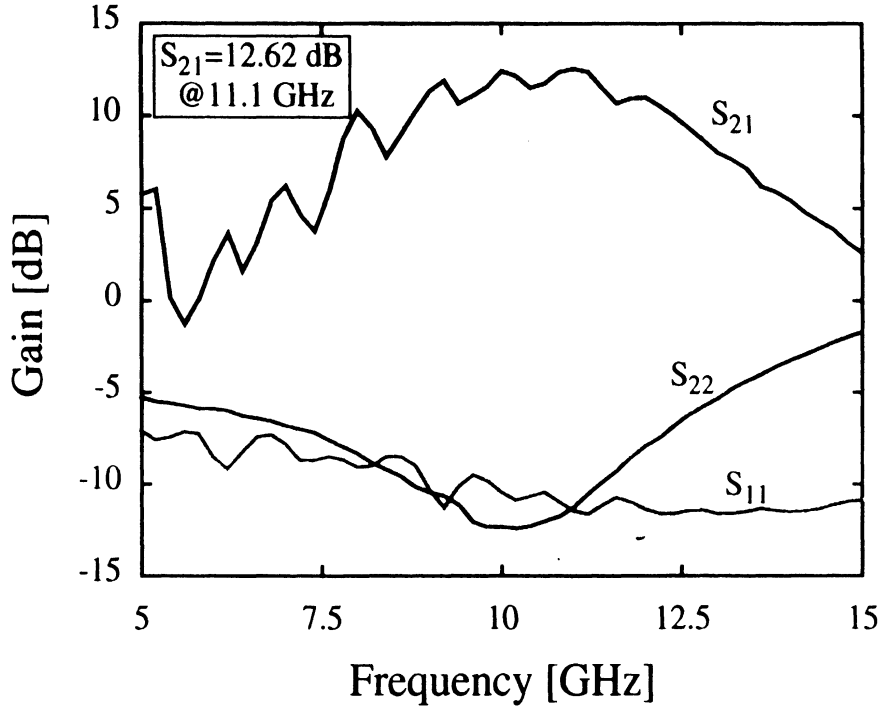

Amplifier Design (Cont'd)

- **Performance of the Single-Stage Amplifier**

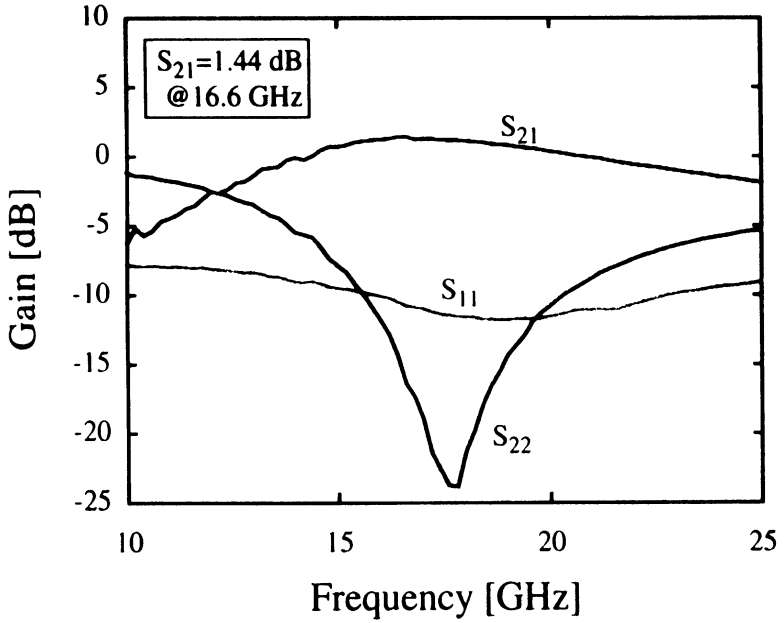

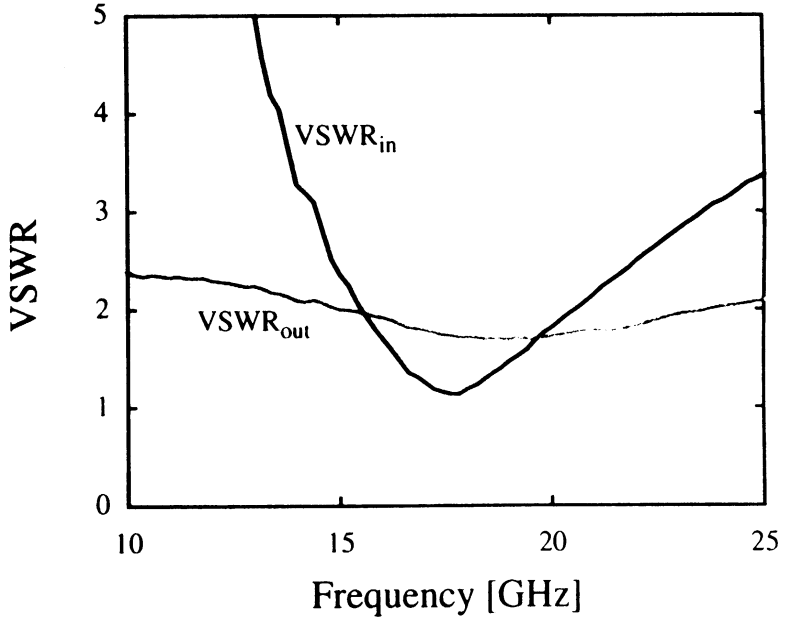

Summary

- Double-mesa structure Si/SiGe HBT with a f_{max} of 52GHz has been fabricated and characterized.
- The resonant frequency of the spiral inductor is improved by a micromachined structure.
- Technologies for Si/SiGe HBTs and micromachined passive components are integrated for Si-based MMIC applications.
- Various amplifiers have been designed and fabricated.